Journal of Computational and Applied Mathematics 462 (2025) 116466

Contents lists available at ScienceDirect

Journal of Computational and Applied Mathematics

journal homepage: www.elsevier.com/locate/cam

Regularity and an adaptive finite element method for elliptic equations with Dirac sources on line cracks

Huihui Cao [a], Hengguang Li [b], Nianyu Yi [c,a], Peimeng Yin [d,*]

[a] School of Mathematics and Computational Science, Xiangtan University, Xiangtan 411105, PR China
[b] Department of Mathematics, Wayne State University, Detroit, MI 48202, USA
[c] Hunan Key Laboratory for Computation and Simulation in Science and Engineering, Xiangtan University, Xiangtan 411105, PR China
[d] Department of Mathematical Sciences, The University of Texas at El Paso, El Paso, TX 79968, USA

ARTICLE INFO

MSC:
65N12
65N30
65N50
35J15

Keywords:
Line Dirac measure
Transmission problem
Regularity
Adaptive finite element method
A posteriori error estimator

ABSTRACT

In this paper, we consider an adaptive finite element method for solving elliptic equations with line Dirac delta functions as the source term. Instead of using a local H^{-1} local indicator, or regularizing the singular source term and using the classical residual-based a posteriori error estimator, we propose a novel a posteriori estimator based on an equivalent transmission problem. This equivalent problem is defined in the same domain as the original problem but features a zero source term and nonzero flux jumps along the line cracks, leading to a more regular solution. The a posteriori error estimator relies on meshes that conform to the line cracks, and its edge jump residual essentially incorporates the flux jumps of the transmission problem on these cracks. The proposed error estimator is proven to be both reliable and efficient. We also introduce an adaptive finite element algorithm based on this error estimator and the bisection refinement method. Numerical tests demonstrate that quasi-optimal convergence rates are achieved for both low-order and high-order approximations, with the associated adaptive meshes primarily refined at a finite number of singular points in the domain.

1. Introduction

We are interested in the adaptive finite element method for the elliptic boundary value problem

$$-\Delta u = \sum_{l=1}^{N} g_l \delta_{\gamma_l} \quad \text{in } \Omega, \qquad u = 0 \quad \text{on } \partial\Omega, \tag{1.1}$$

where $\Omega \subset \mathbb{R}^2$ is a polygonal domain, γ_l, $l = 1, \dots, N$ are line cracks strictly contained in Ω, which may intersect at certain points, as illustrated in Fig. 1(a), $g_l \in H^{\beta_l}(\gamma_l)$ with $\beta_l \geq 0$, and $g_l \delta_{\gamma_l}$ in the source term $\sum_{l=1}^{N} g_l \delta_{\gamma_l}$ is a line Dirac measure on a line crack γ_l, satisfying

$$\langle g_l \delta_{\gamma_l}, v \rangle = \int_{\gamma_l} g_l(s) v(s) ds, \qquad \forall\ v|_{\gamma_l} \in L^2(\gamma_l). \tag{1.2}$$

Although $g_l \in H^{\beta_l}(\gamma_l) \subset L^2(\gamma_l)$, the line Dirac measure $\sum_{l=1}^{N} g_l \delta_{\gamma} \notin L^2(\Omega)$.

The elliptic problem (1.1) is commonly used to describe various phenomena such as monophasic flows in porous media, tissue perfusion, and drug delivery [1]. It also has applications in elliptic optimal control problems [2]. While the solution of the elliptic

* Corresponding author.
E-mail addresses: 201721511145@smail.xtu.edu.cn (H. Cao), li@wayne.edu (H. Li), yinianyu@xtu.edu.cn (N. Yi), pyin@utep.edu (P. Yin).

https://doi.org/10.1016/j.cam.2024.116466
Received 30 July 2024; Received in revised form 8 December 2024
Available online 1 January 2025

problem (1.1) is generally smooth in most of the domain, it becomes singular near the line cracks γ_l and the vertices of the domain [3]. The corner singularity has been well-understood in the literature [4–8] and we will focus on the regularity of the solution near line cracks γ_l. The smoothness of the source term can be obtained through the duality argument [9]. Therefore, the regularity of the solution to problem (1.1) can be derived using the standard elliptic regularity theory [10,11].

Finite element methods for elliptic equations with singular source terms have a long history dating back to the 1970s. However, the primary focus was on point Dirac delta sources [12–18]. More recently, there has been increased attention on singular sources on complex geometries [1–3,19–22], including one-dimensional (1D) crack sources. In [19], the finite element method was studied for problems involving a C^2 closed crack strictly contained in the domain, and an adaptive finite element method was proposed to improve the convergence rate. In [2], as a controlled equation in an optimal control problem, the elliptic problem (1.1) with a single C^2 curve crack was solved using the linear finite element method.

The standard finite element method applied to problem (1.1) can only achieve a convergence rate of $h^{\frac{1}{2}}$ on quasi-uniform meshes due to the lack of regularity. To improve the convergence rate, Li et al. [3] studied the regularity of the solution in a weighted Sobolev space and developed an optimal graded finite element algorithm that approximates the singular solution at an optimal convergence rate on graded meshes. These meshes are densely refined only at the endpoints of the line cracks. However, as the graded finite element applies to (1.1), the grading parameter utilized to generate the graded meshes depends on the smoothness of the functions g_l. Determining this parameter can be difficult and may vary from case to case for different functions g_l.

Adaptive finite element methods (AFEMs) provide an alternative approach to obtain optimal finite element solutions for problem (1.1), as they are effective numerical techniques for problems involving singularities. AFEMs usually consist of four steps (see e.g., [23,24]),

$$\text{SOLVE} \rightarrow \text{ESTIMATE} \rightarrow \text{MARK} \rightarrow \text{REFINE},$$

which generates a sequence of meshes, on which the finite element approximations converge to the solution of the target problem. AFEMs rely on a crucial component: the a posteriori error estimator. This estimator is a computable quantity that depends on both the finite element approximation and known data. It provides information about the size and distribution of the error in the numerical approximation, which can then be used to guide mesh adaptation and as an error estimate. Results on a posteriori error estimates of finite element analysis for second-order elliptic problems with L^2 source terms can be found in [25,26] and the references therein.

Elliptic problems with point Dirac delta source terms have been extensively studied using AFEMs, with residual-based a posteriori error estimators widely employed to guide mesh adaptation and estimate the finite element solution error [23,26–29]. Since the Dirac delta source term has a singularity, it is typically regularized to an $L^2(\Omega)$ or $L^p(\Omega)$ function with $1 < p < \infty$ by projecting the source term to a polynomial space. As a result, the standard residual-based a posteriori error estimator for the general Poisson problems [25,30] can be applied.

For elliptic problems with line Dirac delta source terms, a local data indicator was introduced in [31]. However, it is not easy to compute in practice since it involves a local H^{-1} norm, and the evaluation of the local data indicator for high-order approximations remains an open issue. More recently, regularization techniques have been introduced in studies such as [20,32], which involve projecting the source term to an $L^2(\Omega)$ or $L^p(\Omega)$ function. This allows for the use of standard a posteriori error estimators. The regularization techniques work well for elliptic problems with closed smooth cracks. However, if the cracks are segments, they cannot well reflect the singularity of the solution at the crack endpoints, see Example 4.3.

The solution of (1.1) is continuous throughout the entire domain Ω, but its normal derivative across each line crack shows jumps. Therefore, we resort to investigating an equivalent elliptic problem with a zero source term and nonzero flux jumps on line cracks γ_l. More specifically, the coefficients g_l in the line Dirac source term of (1.1) are transferred to the flux jumps on line cracks of the new problem, which is known as the transmission problem [8]. The transmission problem is defined in the same domain as the original problem, except on the line cracks, along which features a zero source term and nonzero flux jumps. The solution of the elliptic problem (1.1) solves the transmission problem, while the solution of the transmission problem is shown to be more regular, which implies that the finite element solution for problem (1.1) would have a higher convergence rate if the mesh conforms to the line cracks. We also investigate the finite element approximations on quasi-uniform meshes conforming to the line cracks and show the error estimates of the finite element approximations. The convergence rates vary depending on the smoothness of the extended functions of g_l.

Our residual-based a posteriori error estimator is proposed based on the transmission problem. First, we triangulate the mesh conforming to line cracks γ_l, where γ_l is the union of some edges in the triangulation. Second, the error estimator consists of two types of residuals: element residuals with zero source and edge residuals based on the difference between the normal derivative jumps of the FEM solution and the flux jumps (equal to g_l) on line cracks. We derive the reliability and efficiency of the proposed a posteriori error estimator with new techniques for handling the edge residual. Based on the derived error estimator and the bisection mesh refinement method, we propose an adaptive finite element algorithm. Quasi-optimal convergence rates can be numerically achieved for finite element approximations, and the adaptive meshes are primarily refined near the endpoints of line cracks and the singular corners of the domain.

Compared to existing numerical methods, the proposed approach offers several advantages. Firstly, it can effectively capture the most singular part of the solution in the domain, primarily refining the mesh near the endpoints of line cracks and the singular corners of the domain. Secondly, the proposed method is independent of the smoothness of the function g_l, whereas the graded finite element method require knowledge of the smoothness of g_l to determine the grading parameter. More specifically, the contributions, innovations, and significance of this work include:

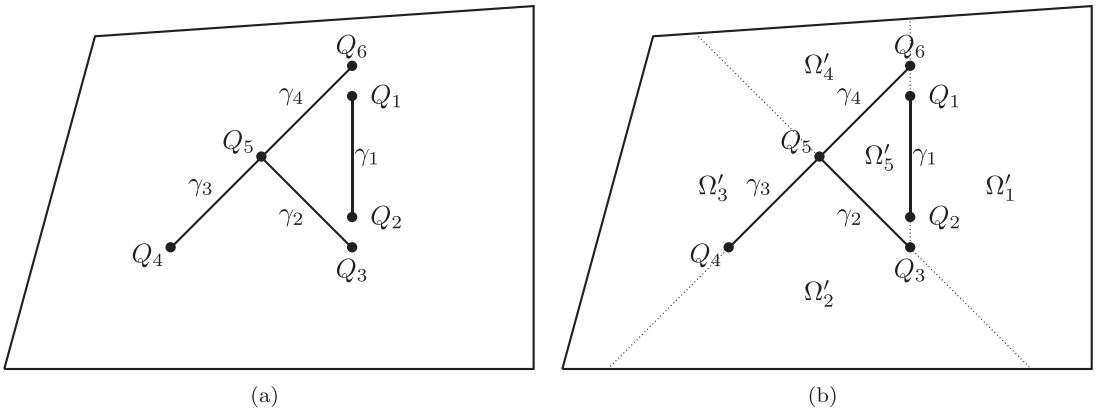

Fig. 1. (a) Domain Ω containing four line cracks γ_1, γ_2, γ_3 and γ_4. (b) Ω is decomposed into five sub-domains $\{\Omega'_j\}_{j=1}^5$ by γ_i, $i = 1, 2, 3, 4$.

- To construct a posteriori error estimator for elliptic boundary value problem (1.1) with a Dirac source term on cracks, we resort to an equivalent transmission problem, which features a zero source term, a zero boundary condition, and an interface condition on the cracks.
- We study the regularity of the elliptic boundary value problem (1.1) in domain Ω and the set $\Omega \setminus \cup_{l=1}^N \gamma_l$, respectively. We show the regularity of the solution in the set $\Omega \setminus \cup_{l=1}^N \gamma_l$ through the transmission problem.
- Based on the a posteriori error estimator and the bisection refinement technique, we propose an adaptive finite element algorithm.
- We rigorously derive the reliability and efficiency of the proposed a posteriori error estimator, with an emphasis on handling the jump of the normal derivatives on the cracks.
- We conduct several numerical examples to verify the performance of the proposed method. Specifically, we compare the a posteriori error estimator with another a posteriori error estimator based on the regularization technique, demonstrating that the proposed estimator can effectively capture the singularity of the solution near the endpoints of the cracks.

The rest of the paper is organized as follows. In Section 2, we discuss the well-posedness and global regularity of problem (1.1) in the whole domain. In addition, we introduce a transmission problem, and investigate its well-posedness, regularity, and relationship to problem (1.1). In Section 3, we propose a novel residual-based a posteriori error estimator, demonstrate its reliability and efficiency, and present our adaptive finite element algorithm. In Section 4, we present various numerical test results to validate our theoretical findings. Throughout the paper, we use $C > 0$ to denote a generic constant that may vary depending on the computational domain but not on the functions involved and mesh parameters.

2. Well-posedness and regularities

Denote by $H^m(\Omega)$, $m \in \mathbb{Z}_{\geq 0}$, the Sobolev space that consists of functions whose ith $(0 \leq i \leq m)$ derivatives are square integrable. Denote by $H_0^1(\Omega) \subset H^1(\Omega)$ the subspace consisting of functions with zero trace on the boundary $\partial\Omega$. For $s > 0$, let $s = m+t$, $0 < t < 1$. Recall that for $D \subseteq \mathbb{R}^d$ for $d = 1, 2$, the fractional order Sobolev space $H^s(D)$ consists of distributions v in D satisfying

$$\|v\|_{H^s(D)}^2 := \|v\|_{H^m(D)}^2 + \sum_{|\alpha|=m} \int_D \int_D \frac{|\partial^\alpha v(x) - \partial^\alpha v(y)|^2}{|x-y|^{d+2t}} dx dy < \infty,$$

where $\alpha = (\alpha_1, \ldots, \alpha_d) \in \mathbb{Z}_{\geq 0}^d$ is a multi-index such that $\partial^\alpha = \partial_{x_1}^{\alpha_1} \ldots \partial_{x_d}^{\alpha_d}$ and $|\alpha| = \sum_{i=1}^d \alpha_i$. We denote by $H_0^s(D)$ the closure of $C_0^\infty(D)$ in $H^s(D)$, and $H^{-s}(D)$ the dual space of $H_0^s(D)$. Let $\gamma \subset \mathbb{R}^1$ be a smooth curve with two endpoints and $\widetilde{H}^s(\gamma)$ be the space of all v defined in γ such that $\tilde{v} \in H^s(\mathbb{R}^1)$, where $\tilde{v}$ is the extension of v by zero outside γ.

2.1. Trace estimates

A sketch drawing of the domain Ω with several line cracks is provided in Fig. 1(a). To obtain the trace estimates on line cracks, we first introduce the trace estimate on a general polygonal domain with no line cracks.

Lemma 2.1 ([33,34]). *Let Ω' be a polygonal domain with no line crack, then the trace operator*

$$\vartheta : H^s(\Omega') \to H^{s-\frac{1}{2}}(\partial\Omega')$$

is bounded for $\frac{1}{2} < s < \frac{3}{2}$.

Lemma 2.2. *For the domain Ω with line segment cracks γ_l, $l = 1, \dots, N$, the trace operator*

$$\vartheta \ : \ H^s(\Omega) \ \to \ H^{s-\frac{1}{2}}(\gamma_l),$$

is bounded for $\frac{1}{2} < s < \frac{3}{2}$.

Proof. By appropriately extending line cracks γ_l, $l = 1, \dots, N$, to the boundary of the domain Ω or to another line crack and denoting the extended line cracks by γ_i', $i = 1, \dots, N'$, we can partition the domain Ω into M polygonal subdomains Ω_j', $1 \le j \le M$, where γ_l' is shared by neighboring subdomains Ω_i' and Ω_j' (see Fig. 1(b)). For any $v \in H^s(\Omega)$, it holds

$$v \in H^s(\Omega_j'), \quad j = 1, \dots, M.$$

By Lemma 2.1, if $\frac{1}{2} < s < \frac{3}{2}$, it follows for $l = 1, \dots, N$,

$$\|v\|_{H^{s-\frac{1}{2}}(\gamma_l)} \le \|v\|_{H^{s-\frac{1}{2}}(\gamma_l')} \le C\|v\|_{H^s(\cup_{j=1}^M \Omega_j')} = C\|v\|_{H^s(\Omega)}.$$

Therefore, the conclusion holds. □

2.2. Well-posedness and regularity in Ω

To investigate the well-posedness and regularity of elliptic problem (1.1), it is necessary to study the line Dirac measure $\sum_{l=1}^N g_l \delta_{\gamma_l}$.

Lemma 2.3. *For $\epsilon > 0$, the line Dirac measure $\sum_{l=1}^N g_l \delta_{\gamma_l} \in H^{-\frac{1}{2}-\epsilon}(\Omega)$ satisfying*

$$\left\| \sum_{l=1}^N g_l \delta_{\gamma_l} \right\|_{H^{-\frac{1}{2}-\epsilon}(\Omega)} \le C \sum_{l=1}^N \|g_l\|_{L^2(\gamma_l)}.$$

Proof. For $v \in H^{\frac{1}{2}+\epsilon}(\Omega)$, by Hölder's inequality and Lemma 2.2, we have for $l = 1, \dots, N$,

$$\langle g_l \delta_{\gamma_l}, v \rangle = \int_{\gamma_l} g_l(s) v(s) ds \le C\|g_l\|_{L^2(\gamma_l)} \|v\|_{L^2(\gamma_l)} \le C\|g_l\|_{L^2(\gamma_l)} \|v\|_{H^\epsilon(\gamma_l)} \le C\|g_l\|_{L^2(\gamma_l)} \|v\|_{H^{\frac{1}{2}+\epsilon}(\Omega)}.$$

Therefore, by the duality argument (e.g., [9])

$$\left\| \sum_{l=1}^N g_l \delta_{\gamma_l} \right\|_{H^{-\frac{1}{2}-\epsilon}(\Omega)} := \sup \left\{ \left\langle \sum_{l=1}^N g_l \delta_{\gamma_l}, v \right\rangle \ : \ \|v\|_{H^{\frac{1}{2}+\epsilon}} = 1 \right\} \le C \sum_{l=1}^N \|g_l\|_{L^2(\gamma_l)}. \quad \square$$

Remark 2.4. Generally, for a function in $H^{\frac{1}{2}}(\Omega)$, its trace on γ_l does not belong to $L^2(\gamma_l)$. Therefore, $\epsilon = 0$ does not hold in Lemma 2.3.

Remark 2.5. The smoothness of $g_l \in H^{\beta_l}(\gamma_l)$ with different $\beta_l \ge 0$ cannot affect the smoothness of $\sum_{l=1}^N g_l \delta_{\gamma_l}$ in Ω, except in the subset $\Omega \setminus \cup_{l=1}^N \gamma_l$, for which we will investigate in the next section.

By Lemma 2.3, the problem (1.1) is well-posed. The variational formulation for problem (1.1) is to find $u \in H_0^1(\Omega)$, such that

$$a(u, v) := \int_\Omega \nabla u \cdot \nabla v dx = \left\langle \sum_{l=1}^N g_l \delta_{\gamma_l}, v \right\rangle, \quad \forall \ v \in H_0^1(\Omega). \tag{2.1}$$

In addition, the following global regularity estimate holds.

Lemma 2.6. *For $\epsilon > 0$, the elliptic boundary value problem (1.1) admits a unique solution $u \in H^{\frac{3}{2}-\epsilon}(\Omega) \cap H_0^1(\Omega)$ satisfying*

$$\|u\|_{H^{\frac{3}{2}-\epsilon}(\Omega)} \le C \sum_{l=1}^N \|g_l\|_{L^2(\gamma_l)}. \tag{2.2}$$

Proof. The standard elliptic theory gives

$$\|u\|_{H^{\frac{3}{2}-\epsilon}(\Omega)} \le C \left\| \sum_{l=1}^N g_l \delta_{\gamma_l} \right\|_{H^{-\frac{1}{2}-\epsilon}(\Omega)} \le C \sum_{l=1}^N \|g_l\|_{L^2(\gamma_l)}.$$

Remark 2.7. The elliptic problem (1.1) is linear, and its solution can be obtained by summing the solutions of the following problems with one line Dirac source term for $l = 1, \dots, N$,

$$-\Delta u_l = g_l \delta_{\gamma_l} \quad \text{in } \Omega, \qquad u_l = 0 \quad \text{on } \partial\Omega. \tag{2.3}$$

By the superposition principle, $u = \sum_{l=1}^{N} u_l$. The regularity estimate in Lemma 2.6 is then obtained by the summation of the regularity estimate $\|u_l\|_{H^{\frac{3}{2}-\epsilon}(\Omega)} \le C_l \|g_l\|_{L^2(\gamma_l)}$ for (2.3) upon using the triangle inequality.

By Lemma 2.6 and the Sobolev imbedding Theorem [34], we have the following result.

Corollary 2.1. *For $\epsilon > 0$, the solution u of problem (1.1) is Hölder continuous $u \in C^{0,1/2-\epsilon}(\Omega)$. In particular, the solution $u \in C^0(\Omega)$.*

Here, Corollary 2.1 implies that the solution of problem (1.1) is continuous across line cracks γ_l, $l = 1, \dots, N$. It is known that for the general elliptic boundary value problem with an $L^2(\Omega)$ source term, the jump of the normal derivative of the solution, also known as flux jumps, on the line cracks vanishes. However, it becomes significant if the problem is subject to line Dirac delta functions. Therefore, it is necessary to study the flux jumps on the line cracks to develop efficient numerical schemes. To this end, we introduce the transmission problem of (1.1) to investigate the normal derivatives of the solution across the line cracks.

2.3. Transmission problem

Let $\mathbf{n}^{\pm}$ be the outward unit normal of the region on each side of the crack γ_l. For a function v, we denote $v^{\pm}$ (resp. $\partial_{\mathbf{n}^{\pm}} v^{\pm}$) the traces of v (resp. ∇v) evaluated on the crack γ_l from the region on each side. We define the jump of v across γ_l by $[v] = v^+ - v^-$ and the jump of its normal derivatives (or flux jumps) on γ_l by $[\partial_{\mathbf{n}} v] = \mathbf{n}^+ \cdot \nabla v^+ + \mathbf{n}^- \cdot \nabla v^-$.

For the elliptic problem (1.1), we introduce the following interface problem,

$$-\Delta w = 0 \quad \text{in } \Omega \setminus \cup_{l=1}^{N} \gamma_l, \tag{2.4a}$$

$$[w] = 0 \quad \text{on } \gamma_l,\ l = 1, \dots, N, \tag{2.4b}$$

$$[\partial_{\mathbf{n}} w] = g_l \quad \text{on } \gamma_l,\ l = 1, \dots, N, \tag{2.4c}$$

$$w = 0 \quad \text{on } \partial\Omega, \tag{2.4d}$$

which is known as the transmission problem of the elliptic problem (1.1) [8]. Compared with the original elliptic problem (1.1), the cracks γ_l, $l = 1, \dots, N$ are treated as the interfaces. Therefore, the jump conditions ((2.4)b) and ((2.4)c) are treated as the interface conditions.

To investigate the solution the of the transmission problem (2.4), we define a space

$$V = \left\{ v \in H^1(\Omega \setminus \cup_{l=1}^{N} \gamma_l) : \ v|_{\partial\Omega} = 0,\ [v]|_{\gamma_l} = 0, \quad l = 1, \dots, N \right\},$$

with the associated norm on V given by

$$\|v\|_V := \|v\|_{H^1(\Omega \setminus \cup_{l=1}^{N} \gamma_l)}, \quad \forall v \in V.$$

Moreover, if $v \in H^1(\Omega)$, then it follows $v \in V$ and $\|v\|_V = \|v\|_{H^1(\Omega)}$.

Lemma 2.8. *The variational formulation for the transmission problem (2.4) is to find $w \in V$ such that*

$$\int_{\Omega \setminus \cup_{l=1}^{N} \gamma_l} \nabla w \cdot \nabla v dx = \sum_{l=1}^{N} \int_{\gamma_l} g_l v ds, \quad \forall v \in H_0^1(\Omega). \tag{2.5}$$

Moreover, it admits a unique solution $w \in V$ satisfying

$$w = u|_{\Omega \setminus \cup_{l=1}^{N} \gamma_l}, \tag{2.6}$$

where u is the solution of the elliptic problem (1.1).

Proof. By multiplying a test function $v \in H_0^1(\Omega)$ on both sides of ((2.4)a), and applying the Green's formula together with the interface and boundary conditions ((2.4)b–d), it follows

$$-\int_{\Omega \setminus \cup_{l=1}^{N} \gamma_l} \Delta w v dx = \int_{\Omega \setminus \cup_{l=1}^{N} \gamma_l} \nabla w \cdot \nabla v dx - \sum_{l=1}^{N} \int_{\gamma_l} [\partial_{\mathbf{n}} w] v ds = 0, \tag{2.7}$$

which gives the variational formulation (2.5).

Since the measure $|\Omega \setminus \cup_{l=1}^{N} \gamma_l| = |\Omega|$, then the variational formulation (2.5) is equivalent to (2.1).

Therefore, the well-posedness of (2.5) or (2.4) follows from that of (2.1) or (1.1). □

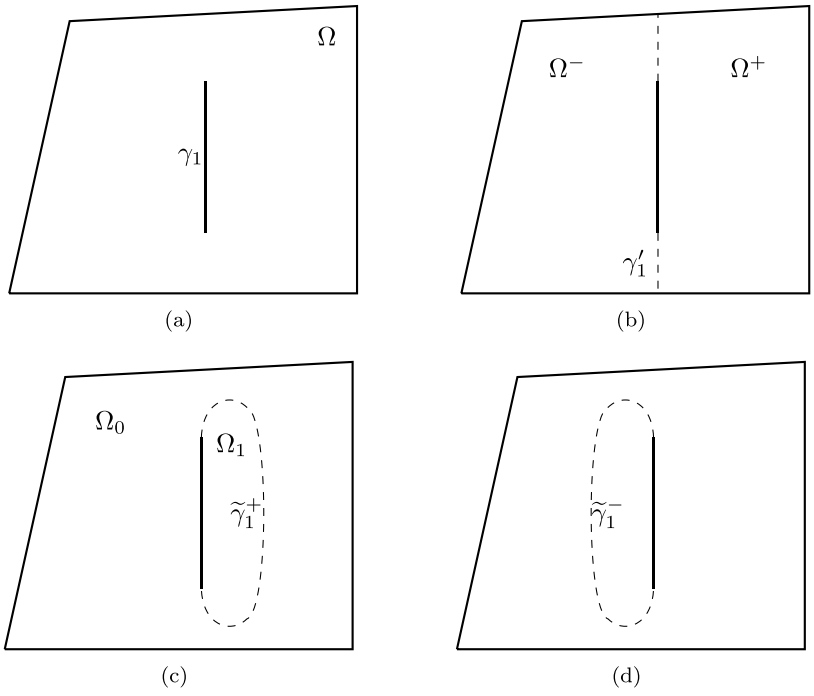

Fig. 2. The extension of the line crack γ_1.

Lemma 2.8 implies that the transmission problem (2.4), admits a unique solution in V. Based on the jump condition ((2.4)b), we can extend it from $\Omega \setminus \cup_{l=1}^{N}\gamma_l$ to the whole domain Ω by taking

$$\bar{w} := \begin{cases} w & \text{in } \Omega \setminus \cup_{l=1}^{N}\gamma_l, \\ w^+(=w^-) & \text{on } \gamma_l,\ l=1,\dots,N. \end{cases} \tag{2.8}$$

Corollary 2.1 and Lemma 2.8 further imply that

$$\bar{w} \in C^0(\Omega) \cap H_0^1(\Omega), \tag{2.9}$$

thus

$$\|\bar{w}\|_{H^1(\Omega)} = \|\bar{w}\|_V = \|w\|_V. \tag{2.10}$$

Therefore, (2.5) is equivalent to the variational formulation

$$a(\bar{w}, v) = \sum_{l=1}^{N} \int_{\gamma_l} g_l v ds, \quad v \in H_0^1(\Omega), \tag{2.11}$$

where the bilinear form $a(\cdot,\cdot)$ is defined in (2.1).

2.4. Regularity in $\Omega \setminus \cup_{l=1}^{N}\gamma_l$

To investigate the regularity of the transmission problem (2.4), we first consider the following interface problem,

$$-\Delta z = 0 \quad \text{in } \Omega \setminus \Gamma_0, \tag{2.12a}$$

$$[z] = 0 \quad \text{on } \Gamma_0, \tag{2.12b}$$

$$[\partial_{\mathbf{n}} z] = g \quad \text{on } \Gamma_0, \tag{2.12c}$$

$$z = 0 \quad \text{on } \partial\Omega, \tag{2.12d}$$

where Γ_0 is a closed sufficiently smooth curve strictly contained in Ω, and $g \in H^{\beta}(\Gamma_0)$ with $\beta \geq 0$. For problem (2.12), we recall the following result from [10,35].

Lemma 2.9. *Let z be the solution of the problem (2.12). Then it follows*

$$\|z\|_{H^{\min\{1+\alpha,\beta+\frac{3}{2}\}}(\Omega\setminus\Gamma_0)} \le C\|g\|_{H^{\beta}(\Gamma_0)}, \tag{2.13}$$

where $\alpha < \frac{\pi}{\omega}$ with ω being the largest interior angle of the polygonal domain Ω.

Next, we introduce the following result from [10, Theorem 1.2.15 and Theorem 1.2.16].

Lemma 2.10. *For a point $x \in \gamma_l$, let $\rho_l(x)$ be multiplication of the distances of x to the endpoints of γ_l. Then*

$$\frac{v}{\rho_l^s} \in L^2(\gamma_l), \qquad \text{if } v \in H^s(\gamma_l) \text{ and } s \in (0, \frac{1}{2});$$
$$\frac{D^\nu v}{\rho_l^{s-|\nu|}} \in L^2(\Omega), \qquad \text{if } v \in H_0^s(\Omega), \quad |\nu| \le s \text{ and } s - \frac{1}{2} \text{ is not an integer.}$$

Recall the definition of the fractional space $\widetilde{H}^s(\gamma_l)$ given at the beginning of Section 2. Then we have the following result.

Lemma 2.11. *For any $\epsilon > 0$, the following statements hold,*

(i) *if $g_l \in H^{\beta_l}(\gamma_l)$, it follows $g_l \in \widetilde{H}^{\min\{\beta_l, \frac{1}{2}-\epsilon\}}(\gamma_l)$;*
(ii) *if $g_l \in H_0^{\beta_l}(\gamma_l)$ and $\beta_l + \frac{1}{2} > 0$ is not an integer, it follows $g_l \in \widetilde{H}^{\beta_l}(\gamma_l)$;*
(iii) *if $g_l \in H_0^{\beta_l}(\gamma_l)$ and $\beta_l + \frac{1}{2} > 0$ is an integer, it follows $g_l \in \widetilde{H}^{\beta_l-\epsilon}(\gamma_l)$.*

Proof. The proofs of (i) and (ii) follow from Lemma 2.10. For (iii), we have $g_l \in H_0^{\beta_l}(\gamma_l) \subset H_0^{\beta_l-\epsilon}(\gamma_l)$, then the conclusion holds by applying Lemma 2.10 and the definition of $\widetilde{H}^s(\gamma_l)$. □

Theorem 2.12. *Recall that $\beta = \min_{1\le l\le N}\{\beta_l\}$ and $\alpha < \frac{\pi}{\omega}$ with ω being the largest interior angle of Ω. For any $\epsilon > 0$, let w be the solution of the transmission problem (2.4). If $g_l \in H^{\beta_l}(\gamma_l)$, $l = 1, \dots, N$, then*

$$\|w\|_{H^{\min\{\alpha+1,\beta+\frac{3}{2},2-\epsilon\}}(\Omega\setminus\cup_{l=1}^N\gamma_l)} \le C\sum_{l=1}^N \|g_l\|_{H^{\beta_l}(\gamma_l)}. \tag{2.14}$$

Further, if $g_l \in H_0^{\beta_l}(\gamma_l)$, $l = 1, \dots, N$, then

$$\begin{aligned}
\|w\|_{H^{\min\{\alpha+1,\beta+\frac{3}{2}\}}(\Omega\setminus\cup_{l=1}^N\gamma_l)} &\le C\sum_{l=1}^N \|g_l\|_{H^{\beta_l}(\gamma_l)}, \quad \text{if } \beta + \tfrac{1}{2} > 0 \text{ is not an integer;} \\
\|w\|_{H^{\min\{\alpha+1,\beta+\frac{3}{2}-\epsilon\}}(\Omega\setminus\cup_{l=1}^N\gamma_l)} &\le C\sum_{l=1}^N \|g_l\|_{H^{\beta_l}(\gamma_l)}, \quad \text{if } \beta + \tfrac{1}{2} > 0 \text{ is an integer.}
\end{aligned} \tag{2.15}$$

Proof. We begin by considering the case with only one line crack γ_1, as illustrated in Fig. 2(a). We extend γ_1 to γ_1', which intersects the boundary $\partial\Omega$ at two points. Consequently, Ω is divided into two open subdomains, Ω^- and Ω^+ (see Fig. 2(b)). Then we prove that the results hold in Ω^- and Ω^+.

In Ω^+, we extend the line crack γ_1 to form a closed C^2 curve $\widetilde{\gamma}_1^+$, further partitioning Ω into two subdomains, Ω_0 and Ω_1, as depicted in Fig. 2(c). Correspondingly, we extend g_1 defined on γ_1 to $\widetilde{g}_1$ defined on $\widetilde{\gamma}_1^+$ as

$$\widetilde{g}_1 = \begin{cases} g_1 & \text{on } \gamma_1, \\ 0 & \text{on } \widetilde{\gamma}_1^+ \setminus \gamma_1. \end{cases} \tag{2.16}$$

Then, the transmission problem (2.4) with $N = 1$ is equivalent to the following interface problem:

$$-\Delta w = 0 \quad \text{in } \Omega \setminus \widetilde{\gamma}_1^+, \tag{2.17a}$$
$$[w] = 0 \quad \text{on } \widetilde{\gamma}_1^+, \tag{2.17b}$$
$$[\partial_{\mathbf{n}} w] = \widetilde{g}_1 \quad \text{on } \widetilde{\gamma}_1^+, \tag{2.17c}$$
$$w = 0 \quad \text{on } \partial\Omega. \tag{2.17d}$$

Note that $\Omega^- \subset \Omega_0$. By Lemmas 2.9 and 2.11, if $g_1 \in H^{\beta_1}(\gamma_1)$, then

$$\begin{aligned}
\|w\|_{H^{\min\{1+\alpha,\beta_1+\frac{3}{2},2-\epsilon\}}(\Omega^-)} &\le \|w\|_{H^{\min\{1+\alpha,\beta_1+\frac{3}{2},2-\epsilon\}}(\Omega_0)} \le C\|\widetilde{g}_1\|_{H^{\min\{\beta_1,\frac{1}{2}-\epsilon\}}(\widetilde{\gamma}_1^+)} \\
&= C\|g_1\|_{\widetilde{H}^{\min\{\beta_1,\frac{1}{2}-\epsilon\}}(\gamma_1)} \le C\|g_1\|_{H^{\beta_1}(\gamma_1)}.
\end{aligned} \tag{2.18}$$

If $g_1 \in H_0^{\beta_1}(\gamma_1)$ and $\beta_1 + \frac{1}{2} > 0$ is not an integer, then

$$\|w\|_{H^{\min\{1+\alpha,\beta_1+\frac{3}{2}\}}(\Omega^-)} \le \|w\|_{H^{\min\{1+\alpha,\beta_1+\frac{3}{2}\}}(\Omega_0)} \le C\|\widetilde{g}_1\|_{H^{\beta_1}(\widetilde{\gamma}_1^+)} = C\|g_1\|_{H^{\beta_1}(\gamma_1)}, \tag{2.19}$$

and if $g_1 \in H_0^{\beta_1}(\gamma_1)$ and $\beta_1 + \frac{1}{2} > 0$ is an integer, then

$$\|w\|_{H^{\min\{1+\alpha,\beta_1+\frac{3}{2}-\epsilon\}}(\Omega^-)} \le \|w\|_{H^{\min\{1+\alpha,\beta_1+\frac{3}{2}-\epsilon\}}(\Omega_0)} \le C\|\widetilde{g}_1\|_{H^{\beta_1-\epsilon}(\widetilde{\gamma}_1^+)} \le C\|g_1\|_{H^{\beta_1}(\gamma_1)}. \tag{2.20}$$

Similarly, we can extend the line crack γ_1 to a closed sufficiently smooth curve $\widetilde{\gamma}_1^-$ in Ω^- as shown in Fig. 2(d) and obtain similar estimates on Ω^+. It can be observed that w is smooth in the neighborhood of $\gamma_1' \setminus \gamma_1$. Thus, if $g_1 \in H^{\beta_1}(\gamma_1)$, then

$$\|w\|_{H^{\min\{1+\alpha,\beta_1+\frac{3}{2},2-\epsilon\}}(\Omega\setminus\gamma_1)} \le C\|g_1\|_{H^{\beta_1}(\gamma_1)}; \tag{2.21}$$

and if $g_1 \in H_0^{\beta_1}(\gamma_1)$, then

$$\begin{aligned} \|w\|_{H^{\min\{1+\alpha,\beta_1+\frac{3}{2}\}}(\Omega\setminus\gamma_1)} &\le C\|g_1\|_{H^{\beta_1}(\gamma_1)}, \quad \text{if } \beta_1 + \tfrac{1}{2} > 0 \text{ is not an integer,} \\ \|w\|_{H^{\min\{1+\alpha,\beta_1+\frac{3}{2}-\epsilon\}}(\Omega\setminus\gamma_1)} &\le C\|g_1\|_{H^{\beta_1}(\gamma_1)}, \quad \text{if } \beta_1 + \tfrac{1}{2} > 0 \text{ is an integer.} \end{aligned} \tag{2.22}$$

We can apply the regularity estimate (2.21) or (2.22) to the case of multiple line cracks and obtain the estimate (2.14) or (2.15) by using the superposition principle, as discussed in Remark 2.7. □

Theorem 2.13. *Let u be the solution of problem (1.1), and w be the solution of the transmission problem (2.4), then it follows*

$$u - \bar{w} \equiv 0 \quad \text{in } \Omega, \tag{2.23}$$

where $\bar{w}$ is the extended solution of w in Ω by (2.8).

Proof. Define the neighborhood of the line crack γ_l as

$$R_\epsilon(\gamma_l) := \{x \in \Omega \mid dist(x, \gamma_l) \le \epsilon\}, \qquad l = 1, \dots, N.$$

Let $R_\epsilon = \cup_{l=1}^N R_\epsilon(\gamma_l)$ and $\Omega = R_\epsilon \cup (\Omega \setminus R_\epsilon)$. We denote the unit outward norm vector of $\Omega \setminus R_\epsilon$ (inward for R_ϵ) on ∂R_ϵ by $\mathbf{n}_\epsilon$.

For any $v \in C_0^\infty(\Omega)$,

$$\begin{aligned} -\int_\Omega \Delta\bar{w} v dx &= -\left(\int_{\Omega\setminus R_\epsilon} \Delta w v dx + \int_{R_\epsilon} \Delta\bar{w} v dx\right) = -\int_{R_\epsilon} \Delta\bar{w} v dx \\ &= \int_{\partial R_\epsilon} \partial_{\mathbf{n}_\epsilon} w v ds + \int_{R_\epsilon} \nabla\bar{w}\nabla v dx. \end{aligned} \tag{2.24}$$

where we have used ((2.4)a) in the second equality, namely, $\Delta w = 0$ in $\Omega \setminus R_\epsilon \subset \Omega \setminus \cup_{l=1}^N \gamma_l$, and Green's formula in the third equality.

By Cauchy–Schwarz inequality, Lemma 2.8 and, the boundedness of ∇v,

$$\left|\int_{R_\epsilon} \nabla\bar{w}\nabla v dx\right| \le \|\nabla\bar{w}\|_{L^2(R_\epsilon)}\|\nabla v\|_{L^2(R_\epsilon)} \le \|\nabla\bar{w}\|_{L^2(\Omega)}\|\nabla v\|_{L^\infty(\Omega)}|R_\epsilon|^{\frac{1}{2}} \to 0, \quad \text{as } \epsilon \to 0,$$

where $|R_\epsilon|$ is the area of the region R_ϵ. Therefore, take $\epsilon \to 0$ in (2.24), it follows

$$-\int_\Omega \Delta\bar{w} v dx = \lim_{\epsilon\to 0}\int_{\partial R_\epsilon} \partial_{\mathbf{n}_\epsilon} w v ds. \tag{2.25}$$

Let $\tilde{u} = u - \bar{w}$. Then for any $v \in C_0^\infty(\Omega)$, it holds

$$-\int_\Omega \Delta\tilde{u} v dx = -\int_\Omega \Delta u v dx + \int_\Omega \Delta\bar{w} v dx = \sum_{l=1}^N \int_{\gamma_l} g_l v ds - \lim_{\epsilon\to 0}\int_{\partial R_\epsilon} \partial_{\mathbf{n}_\epsilon} w v ds = 0, \tag{2.26}$$

where we have used (1.1) for the first term and (2.25) for the second term in the second equality, and

$$\lim_{\epsilon\to 0}\int_{\partial R_\epsilon} \partial_{\mathbf{n}_\epsilon} w v ds = \sum_{l=1}^N \int_{\gamma_l} [\partial_{\mathbf{n}} w] v ds = \sum_{l=1}^N \int_{\gamma_l} g_l v ds.$$

Since v is arbitrary, (2.26) implies

$$-\Delta\tilde{u} = 0 \quad \text{in } \Omega,$$

which together with the boundary condition, $\tilde{u} = u - \bar{w} = 0$ on $\partial\Omega$, yields $\tilde{u} \equiv 0$ in Ω. □

Corollary 2.2. *Recall α, β are given in Theorem 2.12. For any $\epsilon > 0$, it holds:*
(i) Let u be the solution of problem (1.1), then $w = u|_{\Omega\setminus\cup_{l=1}^N \gamma_l}$ solves the transmission problem (2.4);
(ii) If $g_l \in H^{\beta_l}(\gamma_l)$, $l = 1, \dots, N$, it follows

$$u \in H^{\frac{3}{2}-\epsilon}(\Omega) \cap H^{\min\{\alpha+1,\beta+\frac{3}{2},2-\epsilon\}}(\Omega \setminus \cup_{l=1}^{N}\gamma_l).$$

Further, if $g_l \in H_0^{\beta_l}(\gamma_l)$, $l = 1, \dots, N$, *it follows*

$$\begin{aligned} &u \in H^{\frac{3}{2}-\epsilon}(\Omega) \cap H^{\min\{\alpha+1,\beta+\frac{3}{2}\}}(\Omega \setminus \cup_{l=1}^{N}\gamma_l), \quad \text{if } \beta+\tfrac{1}{2} > 0 \text{ is not an integer},\\ &u \in H^{\frac{3}{2}-\epsilon}(\Omega) \cap H^{\min\{\alpha+1,\beta+\frac{3}{2}-\epsilon\}}(\Omega \setminus \cup_{l=1}^{N}\gamma_l), \quad \text{if } \beta+\tfrac{1}{2} > 0 \text{ is an integer}. \end{aligned} \tag{2.27}$$

Proof. The proof follows from Lemmas 2.6, 2.8, Theorems 2.12 and 2.13. □

Remark 2.14. A graded finite element method was proposed for a similar elliptic problem with a single line Dirac delta source δ_{γ_1} in [3]. However, for general $g_l \neq 1$, the grading parameter used to generate the graded meshes depends on the smoothness of the function g_l. Determining this parameter can be challenging and may vary from case to case. In contrast, the AFEM considered in this paper can be applied to general coefficients $g_l \in H^{\beta_l}(\gamma_l)$ with $\beta_l \geq 0$.

Remark 2.15. Theorem 2.12 and Corollary 2.2 remain valid even when γ_l, $l = 1, \dots, N$, are sufficiently smooth curved segments.

3. Adaptive finite element method

In this section, we propose the finite element methods based on the regularity derived in the previous section. Let $\mathcal{T}$ be a shape-regular triangulation of Ω into disjoint elements $\{T\}_{T\in\mathcal{T}}$. Denote the set of edges of $\mathcal{T}$ by $\mathcal{E} = \mathcal{E}_I \cup \mathcal{E}_B$, where $\mathcal{E}_I$ and $\mathcal{E}_B$ represent the set of the interior edges and the boundary edges, respectively. For any triangle $T \in \mathcal{T}$, we denote the diameter of T by h_T.

The Lagrange finite element space is defined by

$$S(\mathcal{T}) = \{v \in C^0(\Omega) \cap H_0^1(\Omega) : v|_T \in P_k(T),\ \forall\, T \in \mathcal{T}\},$$

where $P_k(T)$ denotes polynomials of maximal degree k on T.

Based on the variational formulation (2.1), the standard finite element solution for problem (1.1) is to find $u_h \in S(\mathcal{T})$ such that

$$\int_\Omega \nabla u_h \cdot \nabla v_h dx = \sum_{l=1}^{N} \int_{\gamma_l} g_l(s) v_h(s) ds, \quad \forall\, v_h \in S(\mathcal{T}). \tag{3.1}$$

3.1. Standard finite element method

We suppose that the mesh $\mathcal{T}$ consists of quasi-uniform triangles with mesh size $h := \max h_T$.

Recall that the solution $u \in H^{\frac{3}{2}-\epsilon}(\Omega)$ for any $\epsilon > 0$ (see Lemma 2.6), the standard error estimate [36] on general quasi-uniform meshes, allowing the line cracks pass through the triangles, yields a suboptimal error estimate,

$$\|u - u_h\|_{H^1(\Omega)} \leq C h^{\frac{1}{2}-\epsilon}. \tag{3.2}$$

We further assume the quasi-uniform mesh $\mathcal{T}$ conforming to line cracks γ_l. Namely, γ_l are the union of some edges in $\mathcal{E}_I$ and do not cross with any triangles in $\mathcal{T}$. Recall α, β are given in Theorem 2.12, and the regularity in Corollary 2.2 for u restricted on $\Omega \setminus \cup_{l=1}^{N}\gamma_l$. Then the standard error estimate of the finite element approximations on conforming quasi-uniform meshes gives a better error estimate compared to (3.2). For $\beta_l \geq 0$, if all $g_l \in H^{\beta_l}(\gamma_l)$, then

$$\|u - u_h\|_{H^1(\Omega)} \leq C h^{\min\{\alpha,\beta+\frac{1}{2},1-\epsilon\}}, \tag{3.3}$$

and if all $g_l \in H_0^{\beta_l}(\gamma_l)$, then

$$\begin{aligned} &\|u - u_h\|_{H^1(\Omega)} \leq C h^{\min\{k,\alpha,\beta+\frac{1}{2}\}}, \quad \text{if } \beta+\tfrac{1}{2} > 0 \text{ is not an integer};\\ &\|u - u_h\|_{H^1(\Omega)} \leq C h^{\min\{k,\alpha,\beta+\frac{1}{2}-\epsilon\}}, \quad \text{if } \beta+\tfrac{1}{2} > 0 \text{ is an integer}. \end{aligned} \tag{3.4}$$

From (3.2), (3.3) and (3.4), we can find that the meshes conforming to line cracks gives a better convergence rate. However, no matter whether the meshes conforming to line cracks, the singularity can slow down the convergence of the standard finite element method associated with the quasi-uniform meshes. To further improve the convergence rate, we introduce an adaptive finite element method based on residual type a posteriori error estimator to approximate the solution of problem (1.1).

3.2. Residual-based a posteriori error estimators

We begin by reviewing some existing a posteriori error estimators that can be applied to the elliptic problem (1.1). Following this, we propose a new a posteriori error estimator based on the equivalent transmission problem.

3.2.1. Estimator based on regularization

One way to propose an efficient and reliable residual-based error estimator is to regularize the source term such that the regularized source term belongs to $L^2(\Omega)$ or $L^p(\Omega)$ with $1 < p < \infty$ [20,32]. This allows for the application of the residual-based a posteriori error estimator for the usual Poisson problem. Let $g^r \in L^2(\Omega)$ be a regularized function of the source term $\sum_{l=1}^{N} g_l \delta_{\gamma_l}$ in (1.1), and as $r \to 0$, the solution converges to the exact solution. An example of g^r will be presented in Example 4.3 Test case 1. In turn, the classical residual-based a posteriori error estimator is given by

$$\xi = \left(\sum_{T \in \mathcal{T}} \xi_T^2(u_h) \right)^{\frac{1}{2}}, \tag{3.5}$$

where the local indicator

$$\xi_T(u_h)^2 = h_T^2 \|\Delta u_h + g^r\|_{L^2(T)}^2 + \frac{1}{2} \sum_{e \in \partial T \cap \mathcal{E}_I} h_T \|[\partial_{\mathbf{n}} u_h]\|_{L^2(e)}^2, \tag{3.6}$$

with $[\partial_{\mathbf{n}} u_h]$ being the jump of the normal derivatives of u_h on the interior edges of element T.

The regularization technique is an effective approach for developing an adaptive finite element algorithm that does not require the mesh to conform to line cracks. However, it is important to note that the resulting adaptive finite element solution is subject to both discretization error and regularization error. Moreover, choosing the parameter r in numerical simulations is a nontrivial task. It is sometimes taken as a fixed constant [20], such that the regularization error is comparable to or smaller than the discretization error.

3.2.2. Estimator based on the transmission problem

In this subsection, we mainly introduce an alternative posteriori error estimator, which does not involve the regularized error. Note that each element $T \in \mathcal{T}$ is an open set. We assume that the quasi-uniform mesh $\mathcal{T}$ conforms to line cracks γ_l, namely, each element $T \in \mathcal{T}$ satisfies

$$\gamma_l \cap T = \emptyset, \quad l = 1, \dots, N. \tag{3.7}$$

For analysis convenience, we extend $g_l \in H^{\beta_l}(\Omega)$ from γ_l to $\mathcal{E}_I$ by defining

$$f = \begin{cases} g_l, & e \in \gamma_l, \quad l = 1, \dots, N, \\ 0, & e \in \mathcal{E}_I \setminus \cup_{l=1}^{N} \gamma_l. \end{cases} \tag{3.8}$$

Let $\mathbf{n}$ be the outward unit normal derivative of edge $e \in \mathcal{E}$. By Corollary 2.2, $[\partial_{\mathbf{n}} u] = g_l = f$ for $e \in \gamma_l$, and $[\partial_{\mathbf{n}} u] = 0 = f$ for $e \in \mathcal{E}_I \setminus \cup_{l=1}^{N} \gamma_l$. Therefore, $[\partial_{\mathbf{n}} u]$ is also extended to $\mathcal{E}_I$ in the sense

$$[\partial_{\mathbf{n}} u]|_e = f|_e, \quad e \in \mathcal{E}_I. \tag{3.9}$$

Recall that the transmission problem (2.4) features the interface conditions on the line cracks γ_l, causing the meshes to conform to the line cracks. Based on its equivalence to the elliptic problem (1.1), we propose the following residual-based a posteriori error estimator,

$$\eta = \left(\sum_{T \in \mathcal{T}} \eta_T^2(u_h) \right)^{\frac{1}{2}}, \tag{3.10}$$

where the local indicator on $T \in \mathcal{T}$ is defined by

$$\eta_T(u_h)^2 = h_T^2 \|\Delta u_h\|_{L^2(T)}^2 + \frac{1}{2} \sum_{e \in \partial T \cap \mathcal{E}_I} h_T \|f - [\partial_{\mathbf{n}} u_h]\|_{L^2(e)}^2. \tag{3.11}$$

Before we present the efficiency and reliability of the proposed a posteriori error estimator (3.10), we first prepare some necessary inequalities and estimates.

Lemma 3.1 (*Trace Inequality [37]*). *For any element $T \in \mathcal{T}$, $\forall e \subset \partial T$, we have*

$$\|v\|_{L^2(e)} \le C h_T^{-1/2} (\|v\|_{L^2(T)} + h_T \|\nabla v\|_{L^2(T)}), \qquad \forall v \in H^1(T).$$

Lemma 3.2 (*Inverse Inequality [37]*). *For any element $T \in \mathcal{T}$ and $v \in P_k(T)$, we have*

$$|v|_{H^j(T)} \le C h_T^{-j} \|v\|_{L^2(T)}, \qquad \forall\, 0 \le j \le k.$$

Lemma 3.3 (*Interpolant Error Estimate [37]*). *For any $v \in H^l(T)$, $l \geq 1$, it follows*

$$\|v - \Pi v\|_{H^m(T)} \leq C h^{l-m} \|v\|_{H^l(T)},$$

where $m = 0, 1$ and $\Pi v \in S(\mathcal{T})$ represents the Clément interpolation of v.

In the following analysis, we make use of the equivalence of problem (1.1) to the transmission problem (2.4) as discussed in Section 2.3, and we pay special attention to handle the flux jumps (3.9) on line cracks γ_l in the following reliability analysis.

Theorem 3.4 (*Reliability*). *Assume that u and u_h are the solution of (1.1) and (3.1), respectively. Then the residual-based a posteriori error estimator η satisfies the global bound,*

$$\|\nabla(u - u_h)\|_{L^2(\Omega)} \leq C\eta(u_h). \tag{3.12}$$

Proof. Let $e_u = u - u_h$, we have

$$\|\nabla e_u\|^2_{L^2(\Omega)} = \int_\Omega \nabla e_u \cdot \nabla e_u \, dx = \int_\Omega \nabla e_u \cdot \nabla (e_u - \Pi e_u) \, dx, \tag{3.13}$$

where we have used the Galerkin orthogonality to subtract an interpolant $\Pi e_u \in S(\mathcal{T})$ to e_u. Note that by Corollary 2.2(i) and (3.7), it holds $\Delta u = \Delta w = 0, \ \forall T \in \mathcal{T}$. Therefore,

$$\Delta e_u = \Delta u - \Delta u_h = -\Delta u_h, \quad \text{in each } T \in \mathcal{T}. \tag{3.14}$$

Thus splitting (3.13) into a sum over the elements and using Green's formula, we have

$$\begin{aligned}\sum_{T\in\mathcal{T}} \int_T \nabla e_u \cdot \nabla (e_u - \Pi e_u) \, dx &= \sum_{T\in\mathcal{T}} \int_T -\Delta e_u (e_u - \Pi e_u) \, dx + \int_{\partial T} \mathbf{n} \cdot \nabla e_u (e_u - \Pi e_u) \, ds \\ &= \sum_{T\in\mathcal{T}} \left(\int_T \Delta u_h (e_u - \Pi e_u) \, dx + \int_{\partial T \cap \mathcal{E}_I} \mathbf{n} \cdot \nabla e_u (e_u - \Pi e_u) \, ds \right),\end{aligned}$$

where we have used $\Pi e_u = e_u = 0$ on $\partial\Omega$. Note that e_u is continuous by Corollary 2.1 and the continuity of the finite element solution, so we have $(e_u^+ - \Pi e_u^+)|_e = (e_u^- - \Pi e_u^-)|_e$ for any $e = \partial T^+ \cap \partial T^- \in \mathcal{E}_I$. Thus, it follows

$$\begin{aligned}&\int_{e\cap\partial T^+} \mathbf{n} \cdot \nabla e_u (e_u - \Pi e_u) \, ds + \int_{e\cap\partial T^-} \mathbf{n} \cdot \nabla e_u (e_u - \Pi e_u) \, ds \\ &= \int_e \mathbf{n}^+ \cdot \nabla e_u^+ (e_u^+ - \Pi e_u^+) + \mathbf{n}^- \cdot \nabla e_u^- (e_u^- - \Pi e_u^-) \, ds \\ &= \int_e \left((\mathbf{n}^+ \cdot \nabla u^+ + \mathbf{n}^- \cdot \nabla u^-) - (\mathbf{n}^+ \cdot \nabla u_h^+ + \mathbf{n}^- \cdot \nabla u_h^-) \right) (e_u - \Pi e_u) \, ds \\ &= \int_e [\partial_{\mathbf{n}} u](e_u - \Pi e_u) \, ds - \int_e [\partial_{\mathbf{n}} u_h](e_u - \Pi e_u) \, ds.\end{aligned}$$

This, together with (3.9), implies that

$$\begin{aligned}\sum_{T\in\mathcal{T}} \int_{\partial T\cap\mathcal{E}_I} \mathbf{n} \cdot \nabla e_u (e_u - \Pi e_u) \, ds &= \sum_{e\in\mathcal{E}_I} \left(\int_e [\partial_{\mathbf{n}} u](e_u - \Pi e_u) \, ds - \int_e [\partial_{\mathbf{n}} u_h](e_u - \Pi e_u) \, ds \right) \\ &= \sum_{e\in\mathcal{E}_I} \int_e (f - [\partial_{\mathbf{n}} u_h])(e_u - \Pi e_u) \, ds.\end{aligned}$$

Returning to the sum over the elements with simply distributing half of $f - [\partial_{\mathbf{n}} u_h]$ on T^+ and the remaining half on T^-, we have

$$\|\nabla e_u\|^2_{L^2(\Omega)} = \sum_{T\in\mathcal{T}} \left(\int_T \Delta u_h (e_u - \Pi e_u) \, dx + \frac{1}{2} \sum_{e\in\partial T\cap\mathcal{E}_I} \int_e (f - [\partial_{\mathbf{n}} u_h])(e_u - \Pi e_u) \, ds \right). \tag{3.15}$$

Next, we estimate the terms on the right hand side of (3.15) one by one.

Using Cauchy–Schwarz inequality and Lemma 3.3, we have

$$\int_T \Delta u_h (e_u - \Pi e_u) \, dx \leq \|\Delta u_h\|_{L^2(T)} \|e_u - \Pi e_u\|_{L^2(T)} \leq C h_T \|\Delta u_h\|_{L^2(T)} \|\nabla e_u\|_{L^2(T)}. \tag{3.16}$$

Then, using Cauchy–Schwarz inequality, Lemma 3.1, and Lemma 3.3, we have

$$\begin{aligned}&\int_e (f - [\partial_{\mathbf{n}} u_h])(e_u - \Pi e_u) \, ds \leq \|f - [\partial_{\mathbf{n}} u_h]\|_{L^2(e)} \|e_u - \Pi e_u\|_{L^2(e)} \\ &\quad \leq C \left(h_T^{-1} \|e_u - \Pi e_u\|^2_{L^2(T)} + h_T \|\nabla (e_u - \Pi e_u)\|^2_{L^2(T)} \right)^{1/2} \|f - [\partial_{\mathbf{n}} u_h]\|_{L^2(e)} \\ &\quad \leq C h_T^{1/2} \|f - [\partial_{\mathbf{n}} u_h]\|_{L^2(e)} \|\nabla e_u\|_{L^2(T)}.\end{aligned} \tag{3.17}$$

The estimate (3.12) now follows from (3.15)–(3.17). □

Let $\overline{f} \in P_k(e)$ be the L^2-projection of f. We define the oscillation on $e \in \mathcal{E}_I$ by

$$osc(e)^2 = h_e \|f - \overline{f}\|^2_{L^2(e)},$$

where h_e is the length of e. Let $e = \partial T^+ \cap \partial T^-$ with T^+ and T^- being two adjacent triangles, and we set $\omega_e = T^+ \cup T^-$, then for any $T \in \omega_e$ there exist positive constants C_1 and C_2 such that

$$C_1 h_T \le h_e \le C_2 h_T.$$

For a triangle $T \in \mathcal{T}$ with vertices x_1, x_2, x_3, we denote $(\lambda_{x_1}, \lambda_{x_2}, \lambda_{x_3})$ the barycentric coordinates on T. We define a bubble function b_T in T by

$$b_T = 27\lambda_{x_1}\lambda_{x_2}\lambda_{x_3}. \tag{3.18}$$

For an edge $e = x_i x_j \in \partial T \subset \mathcal{E}$, we define an edge bubble function b_e in T by

$$b_e = 4\lambda_{x_i}\lambda_{x_j}. \tag{3.19}$$

For the bubble functions (3.18) and (3.19), we have the following results.

Lemma 3.5 ([30]). *For the element bubble function b_T in (3.18), it has the following properties,*

$$0 \le b_T(x) \le 1, \quad \forall x \in T, \qquad \text{and} \qquad b_T(x) = 0, \quad \forall x \in \partial T. \tag{3.20}$$

Moreover, for any $v \in P_k$, it follows

$$\|v\|_{L^2(T)} \le C\|b_T^{1/2} v\|_{L^2(T)}. \tag{3.21}$$

Lemma 3.6 ([30]). *For $e = \partial T^+ \cap \partial T^-$, the edge bubble function b_e defined by (3.19) has the following properties,*

$$0 \le b_e(x) \le 1, \quad \forall x \in \omega_e, \qquad \text{and} \qquad b_e(x) = 0, \quad \forall x \in \partial\omega_e \setminus e, \tag{3.22}$$

where $\partial\omega_e = \partial T^+ \cup \partial T^-$. Moreover, for any $v \in P_k$, it follows

$$\|v\|_{L^2(e)} \le C\|b_e^{1/2} v\|_{L^2(e)}, \tag{3.23}$$

$$\|\nabla(b_e v)\|_{L^2(\omega_e)} \le C h_e^{-1/2}\|v\|_{L^2(e)}, \tag{3.24}$$

$$\|b_e v\|_{L^2(\omega_e)} \le C h_e^{1/2}\|v\|_{L^2(e)}. \tag{3.25}$$

Theorem 3.7 (*Efficiency*). *For the local indicator η_T defined in (3.11), it follows*

$$\eta_T(u_h) \le C\left(\|\nabla e_u\|_{L^2(\omega_T)} + osc(\partial T)\right), \quad \forall T \in \mathcal{T}, \tag{3.26}$$

where $\omega_T = \cup_{e\in\partial T}\omega_e$, and

$$osc(\partial T)^2 = \sum_{e\in\partial T} osc(e)^2.$$

Proof. Using Green's formula, (3.14) and (3.20), we have

$$\int_T \nabla e_u \nabla(\Delta u_h b_T)\, dx = -\int_T \Delta e_u\, \Delta u_h b_T\, dx + \int_{\partial T} \nabla e_u \cdot \mathbf{n}\, \Delta u_h b_T\, ds = \int_T \Delta u_h\, \Delta u_h b_T\, dx, \tag{3.27}$$

Since Δu_h is a piecewise polynomial over $\mathcal{T}$, according to (3.21) we have

$$\|\Delta u_h\|^2_{L^2(T)} \le C\|\Delta u_h b_T^{1/2}\|^2_{L^2(T)}.$$

Using the Cauchy–Schwarz inequality, Lemma 3.2, and (3.20), it follows that

$$\begin{aligned}\|\Delta u_h\|^2_{L^2(T)} &\le C\int_T \nabla e_u \nabla(\Delta u_h b_T)\, dx \le C\|\nabla e_u\|_{L^2(T)}\|\nabla(\Delta u_h b_T)\|_{L^2(T)} \\ &\le C h_T^{-1}\|\nabla e_u\|_{L^2(T)}\|\Delta u_h b_T\|_{L^2(T)} \le C h_T^{-1}\|\nabla e_u\|_{L^2(T)}\|\Delta u_h\|_{L^2(T)},\end{aligned}$$

which gives

$$h_T\|\Delta u_h\|_{L^2(T)} \le C\|\nabla e_u\|_{L^2(T)}. \tag{3.28}$$

We now extend $\overline{f}-[\partial_{\mathbf{n}}u_h]$ from edge e to w_e by taking constants along the normal on e. The resulting extension $E(\overline{f}-[\partial_{\mathbf{n}}u_h])$ is a piecewise polynomial in ω_e, then according to (3.24)–(3.25),

$$\|\nabla(E(\overline{f}-[\partial_{\mathbf{n}}u_h])b_e)\|_{L^2(\omega_e)} \le Ch_e^{-\frac{1}{2}}\|\overline{f}-[\partial_{\mathbf{n}}u_h]\|_{L^2(e)}, \tag{3.29}$$

$$\|E(\overline{f}-[\partial_{\mathbf{n}}u_h])b_e\|_{L^2(\omega_e)} \le Ch_e^{\frac{1}{2}}\|\overline{f}-[\partial_{\mathbf{n}}u_h]\|_{L^2(e)}. \tag{3.30}$$

Using arguments similar to those leading to (3.27), it follows

$$\begin{aligned}\int_{\omega_e}\nabla e_u\,\nabla(E(\overline{f}-[\partial_{\mathbf{n}}u_h])b_e)\,dx &= \sum_{T\in\omega_e}\int_T \nabla e_u\,\nabla(E(\overline{f}-[\partial_{\mathbf{n}}u_h])b_e)\,dx\\ &= \sum_{T\in\omega_e}\left(\int_T -\Delta e_u\,E(\overline{f}-[\partial_{\mathbf{n}}u_h])b_e\,dx+\int_{\partial T}\nabla e_u\cdot\mathbf{n}\,E(\overline{f}-[\partial_{\mathbf{n}}u_h])b_e\,ds\right)\\ &= \sum_{T\in\omega_e}\left(\int_T \Delta u_h\,E(\overline{f}-[\partial_{\mathbf{n}}u_h])b_e\,dx+\int_{\partial T}\nabla e_u\cdot\mathbf{n}\,E(\overline{f}-[\partial_{\mathbf{n}}u_h])b_e\,ds\right).\end{aligned}$$

Note that $\overline{f}-[\partial_{\mathbf{n}}u_h]$ and b_e are continuous on $e\in\mathcal{E}_I$, and $b_e=0$ on $\left(\cup_{T\in\omega_e}\partial T\setminus e\right)$, so we have

$$\begin{aligned}&\sum_{T\in\omega_e}\int_{\partial T}\nabla e_u\cdot\mathbf{n}\,E(\overline{f}-[\partial_{\mathbf{n}}u_h])b_e\,ds\\ &= \int_e\left((\mathbf{n}^+\cdot\nabla u^+ + \mathbf{n}^-\cdot\nabla u^-)-(\mathbf{n}^+\cdot\nabla u_h^+ + \mathbf{n}^-\cdot\nabla u_h^-)\right)(\overline{f}-[\partial_{\mathbf{n}}u_h])b_e\,ds\\ &= \int_e[\partial_{\mathbf{n}}u](\overline{f}-[\partial_{\mathbf{n}}u_h])b_e\,ds-\int_e[\partial_{\mathbf{n}}u_h](\overline{f}-[\partial_{\mathbf{n}}u_h])b_e\,ds\\ &= \int_e(f-[\partial_{\mathbf{n}}u_h])(\overline{f}-[\partial_{\mathbf{n}}u_h])b_e\,ds,\end{aligned}$$

where we used (3.9) in the last equality. Therefore, we get

$$\begin{aligned}\int_{\omega_e}\nabla e_u\,\nabla(E(\overline{f}-[\partial_{\mathbf{n}}u_h])b_e)\,dx &= \int_{\omega_e}\Delta u_h\,E(\overline{f}-[\partial_{\mathbf{n}}u_h])b_e\,dx\\ &\quad+\int_e(f-[\partial_{\mathbf{n}}u_h])(\overline{f}-[\partial_{\mathbf{n}}u_h])b_e\,ds\\ &= \int_{\omega_e}\Delta u_h\,E(\overline{f}-[\partial_{\mathbf{n}}u_h])b_e\,dx+\int_e(\overline{f}-[\partial_{\mathbf{n}}u_h])^2b_e\,ds\\ &\quad+\int_e(f-\overline{f})(\overline{f}-[\partial_{\mathbf{n}}u_h])b_e\,ds\end{aligned}$$

It follows from (3.23), we obtain

$$\|\overline{f}-[\partial_{\mathbf{n}}u_h]\|^2_{L^2(e)} \le C\|(\overline{f}-[\partial_{\mathbf{n}}u_h])b_e^{1/2}\|^2_{L^2(e)}.$$

Using Cauchy–Schwarz inequality and (3.29)–(3.30), (3.22), we have

$$\begin{aligned}\|\overline{f}-[\partial_{\mathbf{n}}u_h]\|^2_{L^2(e)} \le& C\left(\int_{\omega_e}\nabla e_u\,\nabla(E(\overline{f}-[\partial_{\mathbf{n}}u_h])b_e)\,dx-\int_{\omega_e}\Delta u_h\,E(\overline{f}-[\partial_{\mathbf{n}}u_h])b_e\,dx\right.\\ &\left.-\int_e(f-\overline{f})(\overline{f}-[\partial_{\mathbf{n}}u_h])b_e\,ds\right)\\ \le& C\left(\|\nabla e_u\|_{L^2(\omega_e)}\|\nabla(E([\overline{f}-\partial_{\mathbf{n}}u_h])b_e)\|_{L^2(\omega_e)}\right.\\ &+\|\Delta u_h\|_{L^2(\omega_e)}\|E([\overline{f}-\partial_{\mathbf{n}}u_h])b_e\|_{L^2(\omega_e)}\\ &\left.+\|(f-\overline{f})b_e\|_{L^2(e)}\|\overline{f}-[\partial_{\mathbf{n}}u_h]\|_{L^2(e)}\right)\\ \le& C\left(h_e^{-1/2}\|\nabla e_u\|_{L^2(\omega_e)}\|\overline{f}-[\partial_{\mathbf{n}}u_h]\|_{L^2(e)}\right.\\ &+h_e^{1/2}\|\Delta u_h\|_{L^2(\omega_e)}\|\overline{f}-[\partial_{\mathbf{n}}u_h]\|_{L^2(e)}\\ &\left.+\|f-\overline{f}\|_{L^2(e)}\|\overline{f}-[\partial_{\mathbf{n}}u_h]\|_{L^2(e)}\right)\\ \le& Ch_e^{-1/2}\|\overline{f}-[\partial_{\mathbf{n}}u_h]\|_{L^2(e)}\left(\|\nabla e_u\|_{L^2(\omega_e)}+h_e\|\Delta u_h\|_{L^2(\omega_e)}+osc(e)\right),\end{aligned}$$

which gives

$$h_e^{\frac{1}{2}}\|\overline{f}-[\partial_{\mathbf{n}}u_h]\|_{L^2(e)} \le C\left(\|\nabla e_u\|_{L^2(\omega_e)}+h_e\|\Delta u_h\|_{L^2(\omega_e)}+osc(e)\right). \tag{3.31}$$

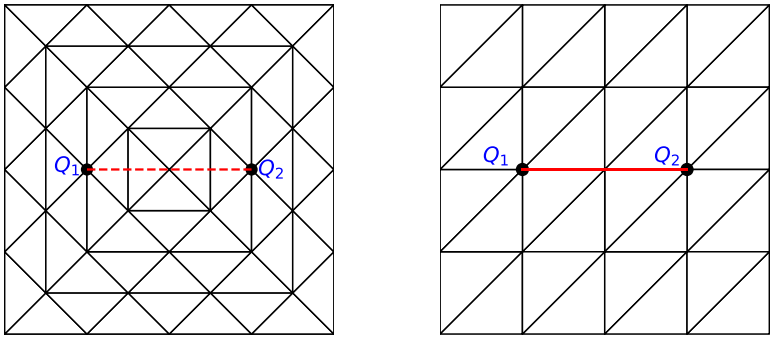

(a) The initial Union-Jack mesh (b) The mesh conforming to γ_1

Fig. 3. Example 4.1: the initial meshes.

Together with the triangle inequality, (3.28) and (3.31), we obtain the estimation

$$h_e^{\frac{1}{2}} \|f - [\partial_{\mathbf{n}} u_h]\|_{L^2(e)} \leq C \left(\|\nabla e_u\|_{L^2(\omega_e)} + osc(e) \right). \tag{3.32}$$

The required estimation now follows form (3.28) and (3.32). □

3.2.3. *Adaptive finite element algorithm*

The adaptive finite element algorithm is based on the general finite element method for problem (1.1), utilizing the error estimator η in (3.10), which is derived from the transmission problem. More specifically, the algorithm is summarized as follows.

Algorithm 3.1 Adaptive finite element algorithm for (1.1).

1: Input: an initial mesh $\mathcal{T}^0$; a constant $0 < \theta < 1$; the maximum number of mesh refinements n.
2: Output: the numerical solution u_h^n; a new refined mesh $\mathcal{T}^n$.
3: for $i = 0$ to n do
  Solve the discrete equation (3.1) for the finite element solution u_h^i on $\mathcal{T}^i$;
  Computing the local error estimation $\eta_T^i(u_h^i)$ and the total error estimation $\eta^i(u_h^i)$ by (3.11) and (3.10);
  if $i < n$ then
    Mark a subset $\widetilde{\mathcal{T}}^i \subset \mathcal{T}^i$ of elements to refined such that
$$\left[\sum_{T \in \widetilde{\mathcal{T}}^i} \eta_T^i(u_h^i)^2 \right]^{1/2} \geq \theta \eta^i(u_h^i);$$
    Refine each element $T \in \widetilde{\mathcal{T}}^i$ by longest edge bisection to obtain a new mesh $\mathcal{T}^{i+1}$.
  end if
end for

Remark 3.8. Both the graded finite element method in [3] and the AFEM considered in this paper are based on the transmission problem. However, the graded finite element method relies on an a priori regularity estimate in a weighted Sobolev space for the transmission problem, whereas the AFEM is based on an a posteriori error estimator derived from the transmission problem.

Remark 3.9. The comparisons of the AFEMs based on different error estimators are presented in Example 4.3. Numerically, the FEM error in the H^1 norm, derived from the *a posteriori* error estimator with regularization ξ in (3.5), achieves only a first-order convergence rate. In contrast, the solution based on η in (3.10), which uses the transmission problem, can achieve arbitrarily high-order convergence.

Remark 3.10. If the line cracks γ_l are curved line segments, we can still introduce a residual-based a posteriori error estimator that does not rely on the regularization techniques by exploring the finite element methods, such as the immersed finite element method [38], and the cut finite element method [39]. For this investigation, we will leave it to our future work.

4. Numerical examples

We present numerical tests for both the finite element method and the adaptive finite element method to validate our theoretical results. All the numerical examples are implemented based on the FEALPY package [40].

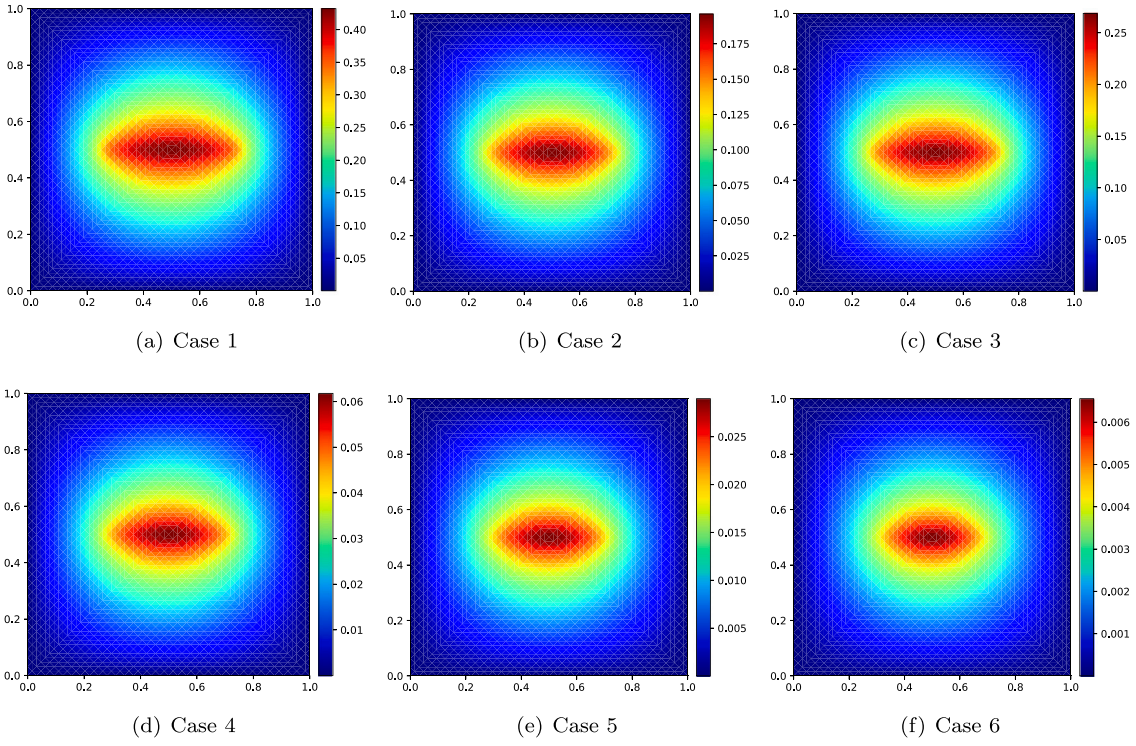

Fig. 4. Test 1: finite element solutions based on P_1 polynomials after 4 mesh refinements.

Table 1
Case 1–6 in Example 4.1.

Case number	r_0	r_1	$g_1 \in$	$u \in$
Case 1	$-\frac{1}{4}+10^{-3}$	1	$H^{\frac{1}{4}}(\gamma_1)$	$H^{\frac{3}{2}-\epsilon}(\Omega)\cap H^{\frac{7}{4}}(\Omega\backslash\gamma_1)$
Case 2	$\frac{1}{4}+10^{-3}$	1	$H^{\frac{1}{4}}(\gamma_1)$	$H^{\frac{3}{2}-\epsilon}(\Omega)\cap H^{2-\epsilon}(\Omega\backslash\gamma_1)$
Case 3	0	1	$C^{\infty}(\gamma_1)$	$H^{\frac{3}{2}-\epsilon}(\Omega)\cap H^{2-\epsilon}(\Omega\backslash\gamma_1)$
Case 4	$\frac{1}{4}+10^{-3}$	0	$H_0^{\frac{1}{4}}(\gamma_1)$	$H^{\frac{3}{2}-\epsilon}(\Omega)\cap H^{\frac{9}{4}}(\Omega\backslash\gamma_1)$
Case 5	$\frac{1}{2}+10^{-3}$	0	$H_0^{1}(\gamma_1)$	$H^{\frac{3}{2}-\epsilon}(\Omega)\cap H^{\frac{5}{2}}(\Omega\backslash\gamma_1)$
Case 6	$1+10^{-3}$	0	$H_0^{\frac{3}{2}}(\gamma_1)$	$H^{\frac{3}{2}-\epsilon}(\Omega)\cap H^{3-\epsilon}(\Omega\backslash\gamma_1)$

4.1. Standard finite element method

In this subsection, we present numerical examples to verify the convergence rate of the standard finite element method solving Eq. (1.1). The quasi-uniform meshes are considered in this subsection, that is, each triangle is divided into four equal triangles in each mesh refinement. Since the solution u is unknown, we use the following numerical convergence rate

$$\mathcal{R} = \log_2 \frac{|u_h^j - u_h^{j-1}|_{H^1(\Omega)}}{|u_h^{j+1} - u_h^j|_{H^1(\Omega)}}, \tag{4.1}$$

where u_h^j is the finite element solution on the mesh $\mathcal{T}^j$ obtained after j refinements of the initial triangulation $\mathcal{T}^0$.

Example 4.1. In this example, we test the convergence rates of the finite element solutions on quasi-uniform meshes. We consider problem (1.1) in a square domain $\Omega = (0,1)^2$ with one line crack $\gamma_1 = Q_1Q_2$ for $Q_1 = (0.25, 0.5)$ and $Q_2 = (0.75, 0.5)$. We take the function $g_1 = ((x-0.25)(0.75-x))^{r_0} + r_1$ on γ_1. For different parameters r_0, r_1 in Case 1–6 listed in Table 1, we show the smoothness of the corresponding function g_1, and the regularity for the solution u of problem (1.1) followed by Corollary 2.2.

Test 1. We take the initial mesh as the Union-Jack mesh and the line crack γ_1 pass through the triangles in the mesh as shown in Fig. 3(a). The convergence rates of the finite element solutions based on P_1, P_2 polynomials are shown in Table 2, and we find that suboptimal convergence rates $\mathcal{R} \approx 0.5$ are obtained for Cases 1–6, which is due to $u \in H^{\frac{3}{2}-\epsilon}(\Omega)$, $\forall \epsilon > 0$ regardless of the smoothness

Table 2
H^1 convergence history of finite element solutions in Example 4.1 Test 1 on Union-Jack meshes.

j	P_1				P_2			
	6	7	8	9	4	5	6	7
Case1	0.477	0.485	0.490	0.493	0.484	0.489	0.493	0.495
Case2	0.475	0.486	0.492	0.496	0.493	0.497	0.498	0.499
Case3	0.485	0.491	0.495	0.497	0.495	0.498	0.499	0.499
Case4	0.476	0.487	0.493	0.496	0.499	0.500	0.500	0.500
Case5	0.476	0.487	0.493	0.497	0.503	0.501	0.500	0.500
Case6	0.474	0.487	0.493	0.497	0.505	0.501	0.500	0.500

Table 3
H^1 convergence history of finite element solutions in Example 4.1 Test 2 on conforming quasi-uniform meshes.

j	P_1				P_2			
	6	7	8	9	5	6	7	8
Case1	0.786	0.786	0.785	0.783	0.792	0.786	0.781	0.777
Case2	0.927	0.937	0.945	0.951	1.045	1.039	1.033	1.028
Case3	0.905	0.916	0.925	0.932	1.000	1.000	1.000	1.000
Case4	0.969	0.979	0.986	0.990	1.253	1.252	1.251	1.251
Case5	0.988	0.994	0.997	0.999	1.500	1.501	1.501	1.501
Case6	0.996	0.999	1.000	1.000	1.865	1.886	1.902	1.914

of g_1 as indicated by Lemma 2.6, and confirms the error estimate (3.2). The contours of the finite element solution for Cases 1–6 are shown in Fig. 4.

Test 2. We take the initial mesh as Fig. 3(b), whose elements conforming to the line crack γ_1. The convergence rates of the finite element solutions based on P_1, P_2 polynomials are shown in Table 3. From the results, we can find that the convergence rates $0.5 < \mathcal{R} < 2$ depends on the smoothness of the function g_1 and the degree of the polynomials. The results in Table 3 satisfy the theoretical expectations shown in Corollary 2.2, and the error estimates (3.3) and (3.4).

The two tests above confirm that the finite element solution on the meshes conforming to the line cracks, namely through the transmission problem, shows better convergence rates than that on meshes with the line crack passing through the triangles.

4.2. Adaptive finite element method

The parameter θ in Algorithm 3.1 is taken as $\theta = 0.25$ in following examples. On adaptive meshes, the convergence rate of the a posteriori error estimator ξ in (3.5) or η in (3.10) for P_k polynomials is called quasi-optimal if

$$\xi \approx N^{-0.5k}, \quad \text{or} \quad \eta \approx N^{-0.5k}.$$

Here and in what follows, we abuse the notation N to represent the total number of degrees of freedom.

Example 4.2. We apply the AFEM to Example 4.1 to test the performance of the proposed a posterior error estimator (3.10) and the corresponding Algorithm 3.1. We take the mesh in Fig. 3(b) as the initial mesh.

The convergence rates of the error estimator η based on P_1 and P_2 polynomials are shown in Fig. 6. From the results, we find that the convergence rates of η are quasi-optimal. The contours of the AFEM approximations for different cases are shown in Fig. 5, from which we can find that these solutions are almost identical to those in Example 4.1 Test 1.

For Cases 1–6, the function g_1 is sufficiently smooth on γ_1 except near the endpoints Q_1 and Q_2 of the line crack γ_1, so the solution is more singular near these two endpoints compared with any other regions in the domain. Figs. 7 and 8 show the adaptive meshes of P_1, P_2 approximations, respectively. We can see clearly that the error estimator guide the mesh refinements densely around the endpoints Q_1 and Q_2. We also find that the more regular the solution is, the less dense the mesh concentrates at the endpoints Q_1 and Q_2. It is worth noting that Case 3 is an example in [3] solved by the graded finite element method, which showed optimal convergence rates with mesh refinements concentrating at the singular points Q_1 and Q_2 as well.

Example 4.3. We consider problem (1.1) on an L-shaped domain $\Omega = (-1,1)^2\backslash[0,1)^2$ and take the line cracks $\cup_{l=1}^6 \gamma_l = \partial\Omega_1$ with $\Omega_1 = (-0.8,-0.2)^2\backslash[-0.5,-0.2)^2$ as shown in Fig. 9(a). The function $g_l = 5$ on γ_l, $l = 1,\dots,6$. We apply the AFEMs based on the residual-based a posteriori error estimators ξ in (3.5) and η in (3.10) to solve this problem, respectively. Both AFEMs take the mesh in Fig. 9(a) as their initial mesh.

Test 1. We first consider the AFEM based on the residual-based a posteriori error estimator ξ in (3.5). For simplicity of presentation, we denote $\gamma = \cup_{l=1}^6 \gamma_l$, and $g|_{\gamma_l} = g_l$, $l = 1,\dots,6$. Instead of directly discretizing (1.1), one discretize its regularized problem, which is to replace the line Dirac source term $\sum_{l=1}^N g_l \delta_{\gamma_l}$ by its regularized data [20],

$$g^r(x) = \int_\gamma g(y)\delta^r(y-x)\,\mathrm{d}y \in L^2(\Omega),$$

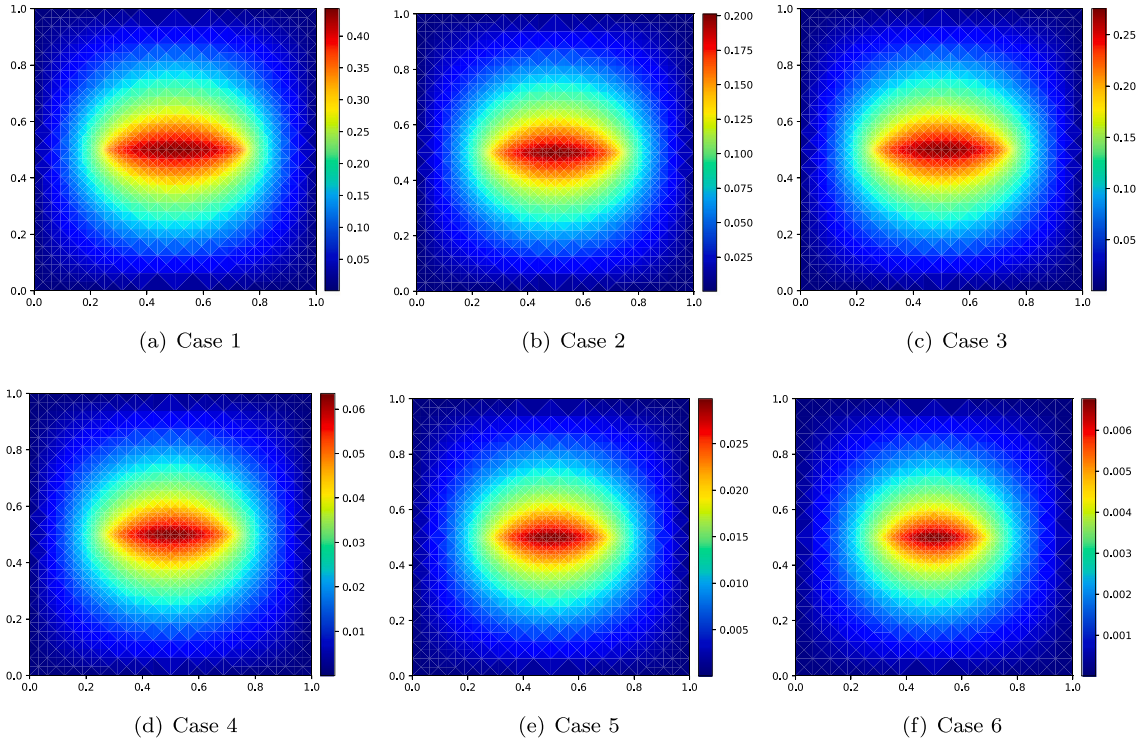

Fig. 5. Example 4.2: AFEM solutions based on P_1 polynomials.

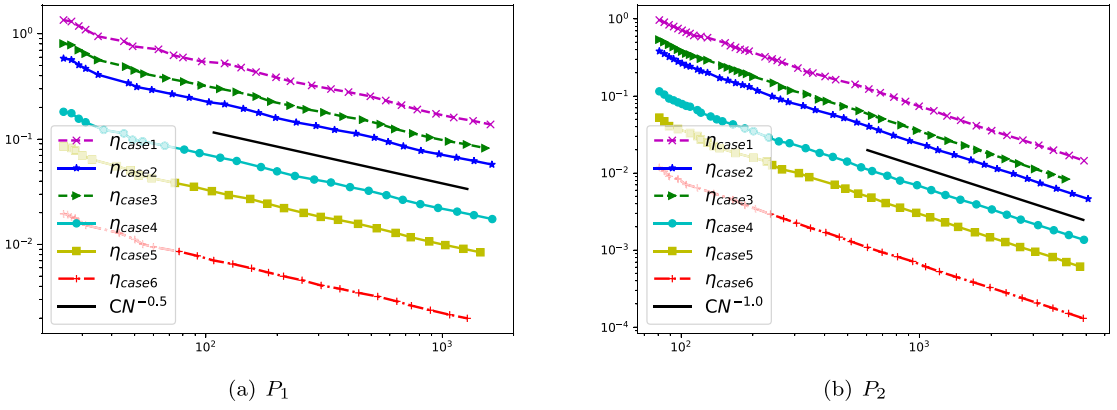

Fig. 6. Example 4.2: error estimators.

where r is the regularization parameter depending on the local mesh size, and the line Dirac approximation δ^r of the Dirac distribution δ is defined by

$$\delta^r(x) = \frac{1}{r^2}\psi\left(\frac{x}{r}\right),$$

with suitable choice of $\psi(x)$ satisfying [20,41,42]

$$\lim_{r\to 0}\delta^r(x) = \lim_{r\to 0}\frac{1}{r^2}\psi\left(\frac{x}{r}\right) = \delta(x),$$

where the limit should be understood in the space of Schwartz distributions [43].

Similar to [20], we take r as a constant in actual numerical simulation. More specifically, we set $r = 0.05$, and

$$\psi(x) = \frac{1}{4}\chi_{[-1,1]}(x_1)\cdot\chi_{[-1,1]}(x_2),$$

where $\chi_{[-1,1]}(x_i)$ is the characteristic function defined by

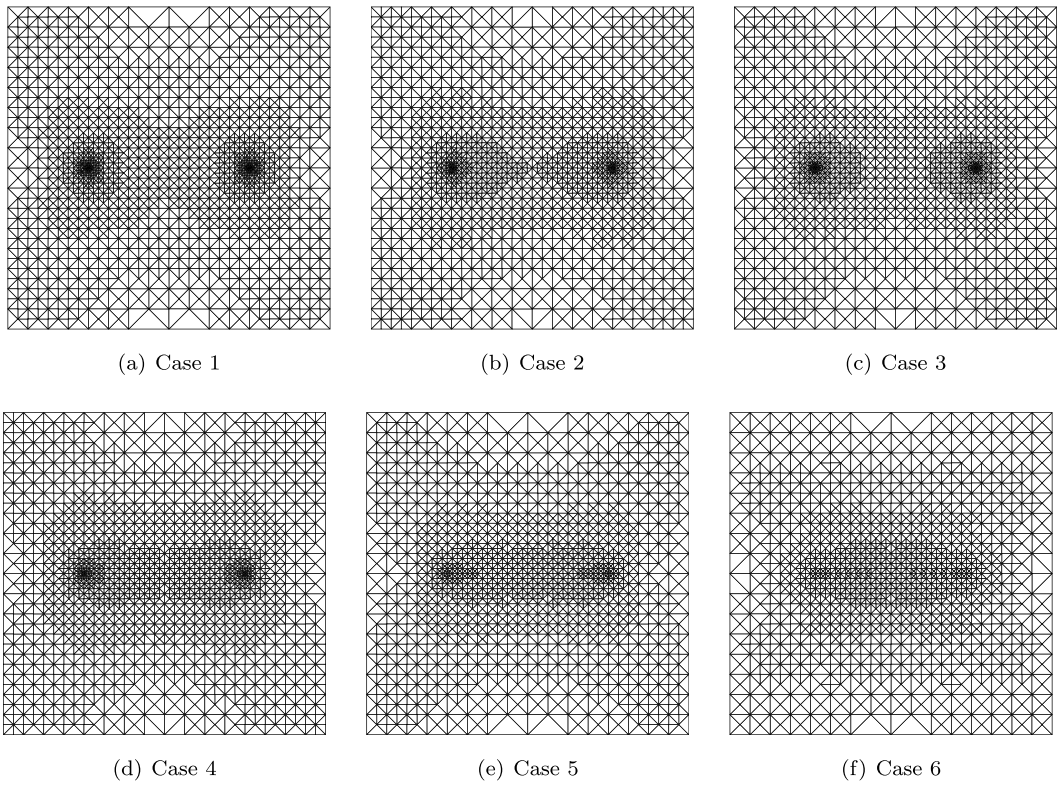

Fig. 7. Example 4.2: adaptive meshes based on P_1 polynomials.

$$\chi_{[-1,1]}(x_i) = \begin{cases} 1, & -1 \le x_i \le 1, \\ 0, & \text{others}. \end{cases}$$

The contour of the AFEM solution with g^r as the source function based on P_1 polynomials is shown in Fig. 9(b).

Test 2. We then consider the AFEM based on the residual-based a posteriori error estimator η in (3.10), namely, the Algorithm 3.1, for problem (1.1). The contour of the AFEM solution based on P_1 polynomials is shown in Fig. 9(c), which is comparable to the contour in Test 1 as shown in Fig. 9(b).

Since $g_l \in C^\infty(\gamma_l)$, the solution is more singular at the endpoints of line cracks γ_l and the reentrant corner of the domain. The adaptive meshes from Test 1 and Test 2 based on P_1 polynomials are shown in Figs. 10(a) and (b), respectively. From the results, we find that both meshes are densely refined at the endpoints of the line cracks γ_l and the reentrant corner of the domain, but the mesh from Test 1 is also densely refined on the whole line cracks γ_l, $l = 1, \dots, 6$. Similar adaptive meshes can also be found for Test 1 and Test 2 based on P_2 polynomials as shown in Fig. 11(a)–(b). These results imply that the error estimator η in (3.10) guides the mesh refinements effectively by only densely refining the triangles around the endpoints of the line cracks, where the solution is more singular.

The convergence rates of the error estimator ξ and η based on P_1 polynomials are shown in Fig. 10(c). We can find that the error estimators from both Test 1 and Test 2 are quasi-optimal with $\xi \approx N^{-0.5}$ and $\eta \approx N^{-0.5}$. The convergence rates based on P_2 polynomials are shown in Fig. 11(c). From the results, we can find that the error estimator $\eta \approx N^{-1}$ for Test 2 is quasi-optimal, but the error estimator $\xi(\approx N^{-0.5})$ for Test 1 does not achieve the quasi-optimal rate even with more dense refined meshes.

Example 4.4. In this example, we first introduce four intersecting line cracks $\gamma_l = QQ_l$, $l = 1, \dots, 4$, where $Q(0.5, 0.5)$, $Q_1(0.25, 0.5)$, $Q_2(0.75, 0.5)$, $Q_3(0.5, 0.25)$ and $Q_4(0.5, 0.75)$. Here, we consider three types of geometries of Ω. Geometry 1 consists of two line cracks γ_2 and γ_4; Geometry 2 consists of three line cracks γ_2, γ_3 and γ_4; Geometry 3 consists of all line cracks γ_l, $l = 1, \dots, 4$. The initial meshes of Geometry 1–3 are shown in Fig. 13. The functions g_l on each line crack γ_l are taken as the following,

$$g_1 = -g_2 = -g_3 = g_4 = -1. \tag{4.2}$$

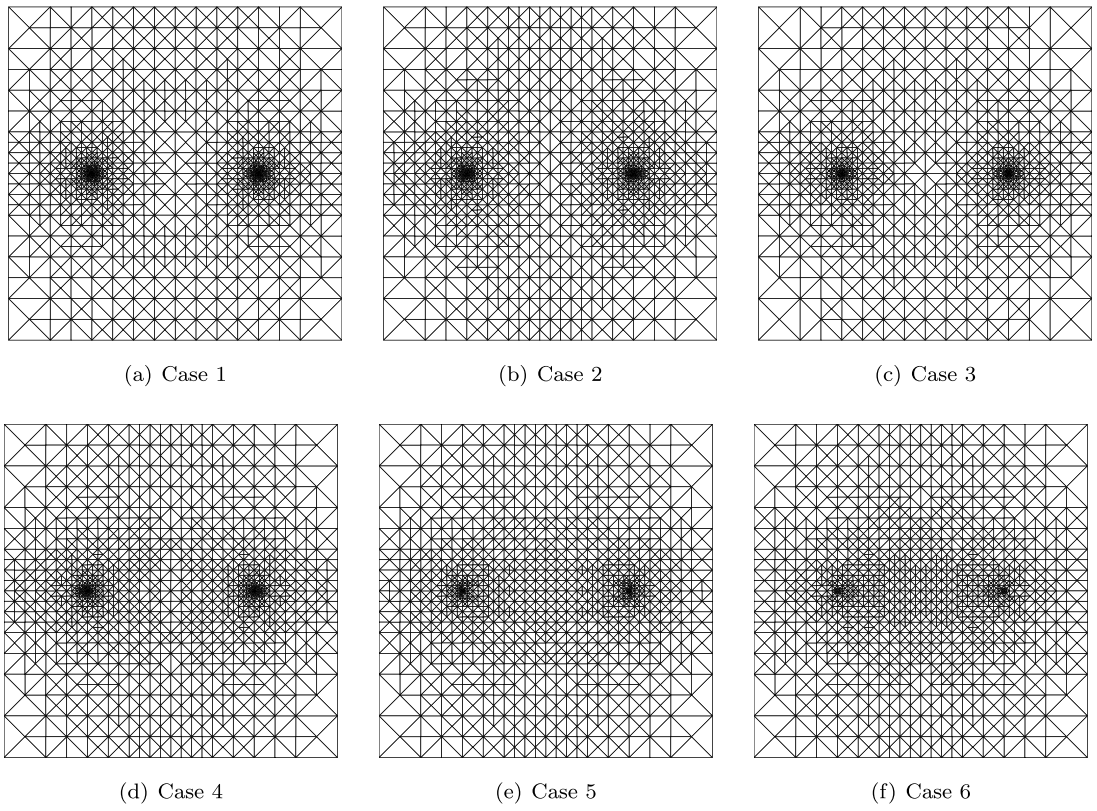

(a) Case 1 (b) Case 2 (c) Case 3

(d) Case 4 (e) Case 5 (f) Case 6

Fig. 8. Example 4.2: adaptive meshes based on P_2 polynomials.

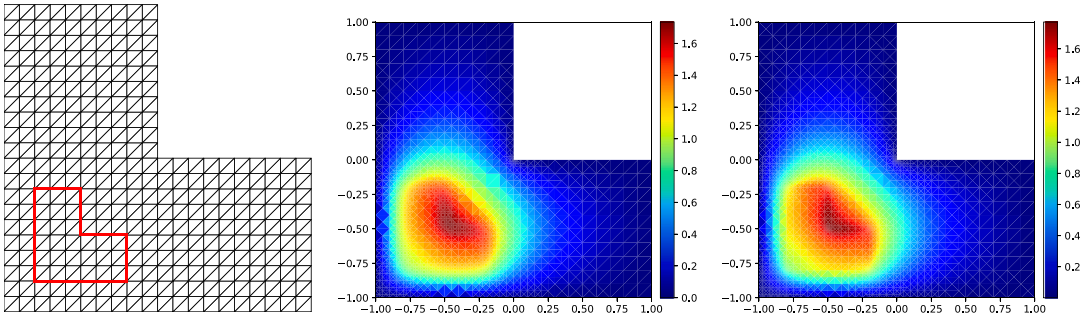

(a) Domain with initial mesh (b) Solution of Test 1 (c) Solution of Test 2

Fig. 9. Example 4.3: Initial mesh and finite element solutions.

The history of the error estimators are reported in Fig. 14, which shows that the convergence rates of the error estimators are quasi-optimal for all the three cases. Figs. 15–16 and Fig. 12 show the corresponding adaptive mesh refinements and the numerical solutions, respectively. We can see clearly that the error estimator successfully guide the mesh refinement around the singular points Q and Q_l, $l = 1, 2, 3, 4$, where the solution shows singularity.

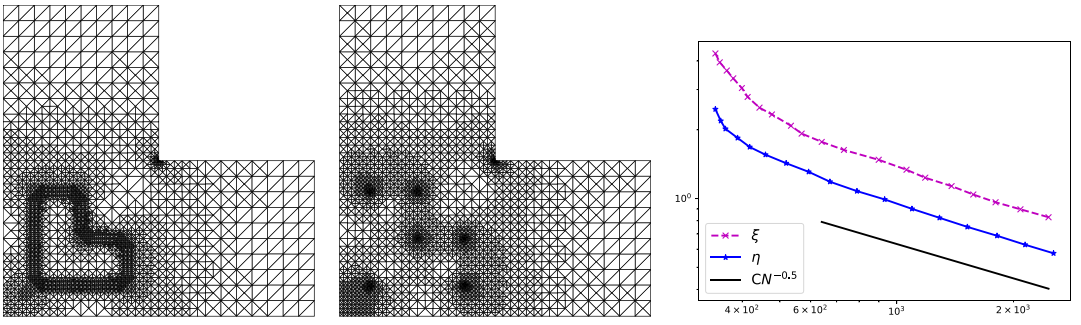

(a) Adaptive mesh of Test 1 (b) Adaptive mesh of Test 2 (c) Error estimators

Fig. 10. Example 4.3: Meshes and estimators based on P_1 polynomials.

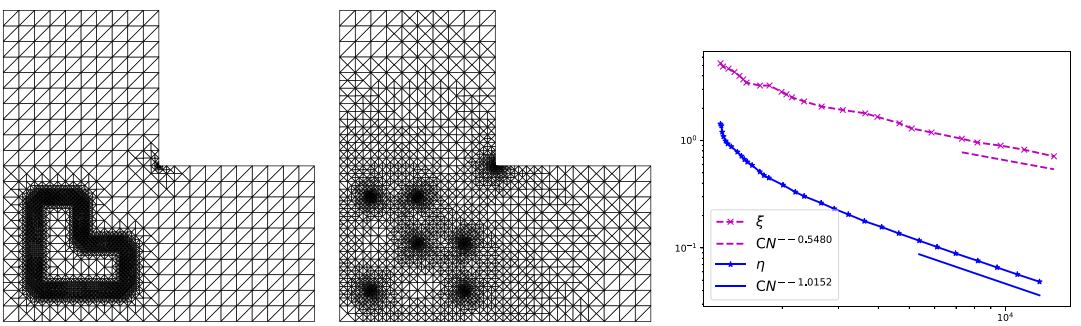

(a) Adaptive mesh of Test 1 (b) Adaptive mesh of Test 2 (c) Error estimators

Fig. 11. Example 4.3: Meshes and estimators based on P_2 polynomials.

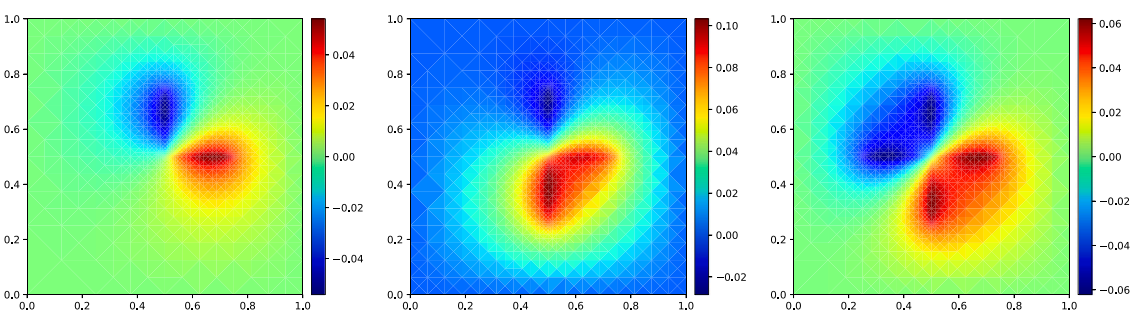

(a) Geometry 1 (b) Geometry 2 (c) Geometry 3

Fig. 12. Example 4.4: AFEM solutions based on P_1 polynomials.

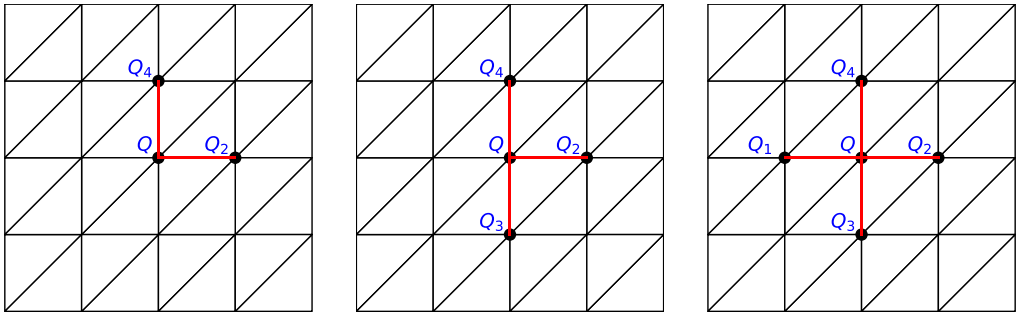

(a) Geometry 1 (b) Geometry 2 (c) Geometry 3

Fig. 13. Example 4.4: initial meshes.

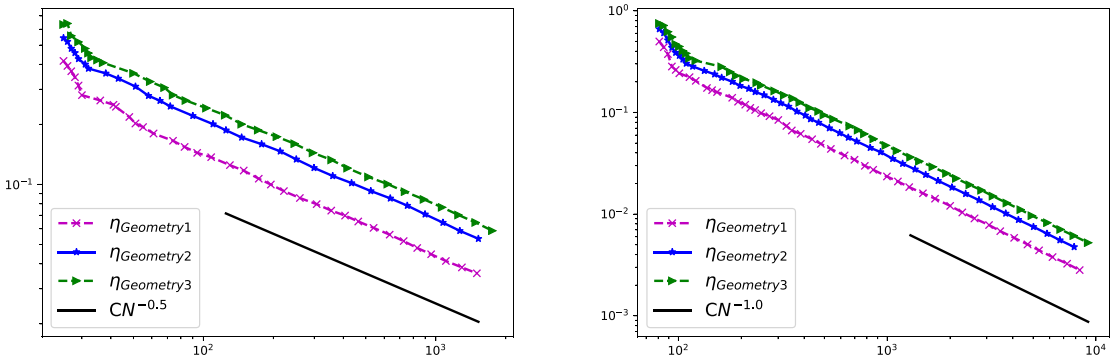

(a) P_1 (b) P_2

Fig. 14. Example 4.4: error estimators.

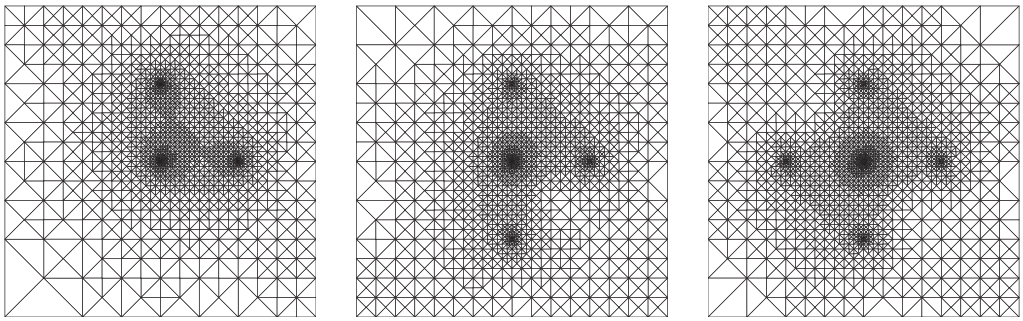

(a) Geometry 1 (b) Geometry 2 (c) Geometry 3

Fig. 15. Example 4.4: adaptive meshes based on P_1 polynomials.

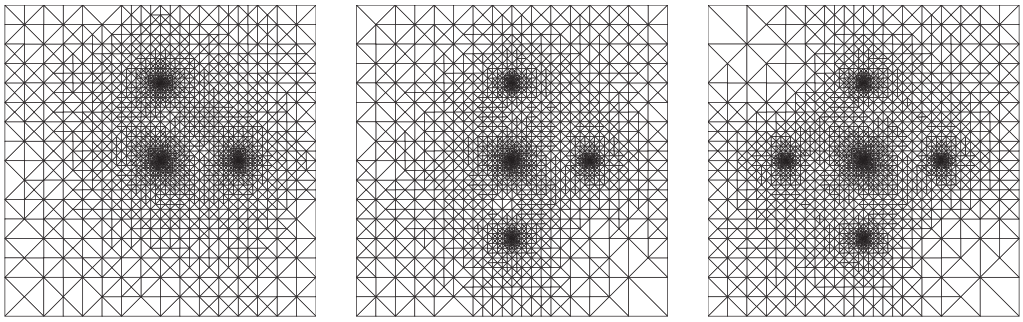

(a) Geometry 1 (b) Geometry 2 (c) Geometry 3

Fig. 16. Example 4.4: adaptive meshes based on P_2 polynomials.

5. Conclusion

In this work, we propose a novel residual-based a posteriori estimator for elliptic problems with line Dirac delta functions. To begin our approach, we first identify an equivalent transmission problem that shares the same solution as the original problem and treats the line cracks as the interfaces. This transmission problem for our case is an interface problem, which has a continuous solution and nonzero flux jumps $[\partial_{\mathbf{n}} u] = g_l$ on the line cracks γ_l. The proposed a posteriori estimator, relying on meshes conforming to the line cracks, consists of element residuals with zero source and edge residuals involving flux jumps g_l. We derive the reliability and efficiency of the a posteriori estimator with the main focus on handling the estimates of the edge residuals. An AFEM is given based on the proposed a posteriori estimator and the bisection refinement method. Our method has some remarkable achievements. We identify the regularities of the original problem in the whole domain and the domain excluding the line cracks. The proposed AFEM can achieve the quasi-optimal convergence rate for both low order and high order approximations. The adaptive meshes are primarily refined at some singular points of the domain, namely, the endpoints of the line cracks and the singular corners of the domain.

Although our investigation currently focuses on line cracks, it has potential to expand the proposed method to more complex cases. In particular, it holds potential for 2D elliptic problems with curved cracks and 3D elliptic problems with surface interfaces strictly contained within the domain. To explore these extensions, we will need to develop new mathematical tools, and it will be the focus of our future work.

Acknowledgments

H. Cao was supported by China's National Key R&D Programs (2020YFA0713500). H. Li was supported in part by the National Science Foundation, United States Grant DMS-2208321 and by the Wayne State University Faculty Competition for Postdoctoral Fellows Award. N. Yi was supported by NSFC Project (12431014, 12261131501). P. Yin was supported by the University of Texas at El Paso Startup Award.

Data availability

Enquiries about data availability should be directed to the authors.

References

[1] C. D'Angelo, Finite element approximation of elliptic problems with Dirac measure terms in weighted spaces: applications to one- and three-dimensional coupled problems, SIAM J. Numer. Anal. 50 (1) (2012) 194–215.
[2] W. Gong, G. Wang, N. Yan, Approximations of elliptic optimal control problems with controls acting on a lower dimensional manifold, SIAM J. Control Optim. 52 (3) (2014) 2008–2035.
[3] H. Li, X. Wan, P. Yin, L. Zhao, Regularity and finite element approximation for two-dimensional elliptic equations with line Dirac sources, J. Comput. Appl. Math. 393 (2021) 113518.
[4] T. Apel, Anisotropic Finite Elements: Local Estimates and Applications, in: Advances in Numerical Mathematics, B. G. Teubner, Stuttgart, 1999.
[5] M. Dauge, Elliptic Boundary Value Problems on Corner Domains, in: Lecture Notes in Mathematics, vol. 1341, Springer-Verlag, Berlin, 1988.
[6] P. Grisvard, Elliptic Problems in Nonsmooth Domains, in: Monographs and Studies in Mathematics, vol. 24, Pitman (Advanced Publishing Program), Boston, MA, 1985.
[7] V. Kondrat'ev, Boundary value problems for elliptic equations in domains with conical or angular points, Trudy Moskov. Mat. Obšč. 16 (1967) 209–292.
[8] H. Li, A. Mazzucato, V. Nistor, Analysis of the finite element method for transmission/mixed boundary value problems on general polygonal domains, Electron. Trans. Numer. Anal. 37 (2010) 41–69.
[9] J. Lions, E. Magenes, Non-Homogeneous Boundary Value Problems and Applications, Vol. 1, Springer-Verlag, 1972.
[10] P. Grisvard, Singularities in Boundary Value Problems, in: Research Notes in Applied Mathematics, vol. 22, Springer-Verlag, New York, 1992.

[11] S. Alinhac, P. Gérard, S.S. Wilson, Pseudo-Differential Operators and the Nash-Moser Theorem, in: Stud. Math., vol. 82, AMS, Providence, RI, 2007.
[12] I. Babuška, Error-bounds for finite element method, Numer. Math. 16 (1971) 322–333.
[13] R. Scott, Finite element convergence for singular data, Numer. Math. 21 (1973) 317–327.
[14] R. Scott, Optimal L^{∞} estimates for the finite element method on irregular meshes, Math. Comp. 30 (1976) 681–697.
[15] E. Casas, L^2 estimates for the finite element method for the Dirichlet problem with singular data, Numer. Math. 47 (1985) 627–632.
[16] R. Araya, E. Behrens, R. Rodríguez, A posteriori error estimates for elliptic problems with Dirac delta source terms, Numer. Math. 105 (2006) 193–216.
[17] P. Houston, T.P. Wihler, Discontinuous Galerkin methods for problems with Dirac delta source, ESAIM Math. Model. Numer. Anal. 46 (6) (2012) 1467–1483.
[18] H. Cao, Y. Huang, N. Yi, Yin. P, A posteriori error estimators for fourth order elliptic problems with concentrated loads, arXiv preprint arXiv:2408.15863 (2025).
[19] L. Heltai, N. Rotundo, Error estimates in weighted Sobolev norms for finite element immersed interface methods, Comput. Math. Appl. 78 (11) (2019) 3586–3604.
[20] L. Heltai, W. Lei, Adaptive finite element approximations for elliptic problems using regularized forcing data, SIAM J. Numer. Anal. 61 (2) (2023) 431–456.
[21] C. D'Angelo, A. Quarteroni, On the coupling of 1D and 3D diffusion-reaction equations. Application to tissue perfusion problems, Math. Models Methods Appl. Sci. 18 (8) (2008) 1481–1504.
[22] S. Ariche, C. De Coster, S. Nicaise, Regularity of solutions of elliptic or parabolic problems with Dirac measures as data, SeMA J. 73 (2016) 379–426.
[23] W. Dörfler, A convergent adaptive algorithm for Poisson equation, SIAM J. Numer. Anal. 33 (3) (1996) 1106–1124.
[24] P. Morin, R. Nochetto, K. Siebert, Convergence of adaptive finite element methods, SIAM Rev. 44 (2002) 631–658.
[25] M. Ainsworth, J.T. Oden, A Posteriori Error Estimation in Finite Element Analysis, Wiley Interscience, New York, 2000.
[26] R. Verfürth, A Review of a Posteriori Error Estimation and Adaptive Mesh-Refinment Techniques, Wiley-Teubner, Chichester, 1996.
[27] P. Binev, W. Dahmen, R. DeVore, Adaptive Finite Element Methods with convergence rates, Numer. Math. 97 (2004) 219–268.
[28] P. Morin, R. Nochetto, K. Siebert, Data oscillation and convergence of adaptive FEM, SIAM J. Numer. Anal. 38 (2) (2000) 466–488.
[29] R. Stevenson, Optimality of a standard adaptive finite element method, Found. Comput. Math. 7 (2) (2007) 245–269.
[30] R. Verfürth, A posteriori error estimation and adaptive mesh-refinement techniques, J. Comput. Appl. Math. 50 (1–3) (1994) 67–83.
[31] A. Cohen, R. DeVore, R.H. Nochetto, Convergence rates of AFEM with H^{-1} data, Found. Comput. Math. 12 (2012) 671–718.
[32] F. Millar, I. Muga, S. Rojas, Projection in negative norms and the regularization of rough linear functionals, Numer. Math. 150 (2022) 1087–1121.
[33] Z. Ding, A proof of the trace theorem of Sobolev spaces on Lipschitz domains, Proc. Amer. Math. Soc. 124 (2) (1996) 591–600.
[34] W. McLean, Strongly Elliptic Systems and Boundary Integral Equations, Cambridge University Press, 2000.
[35] Z. Chen, J. Zou, Finite element methods and their convergence for elliptic and parabolic interface problems, Numer. Math. 79 (2) (1998) 175–202.
[36] Philippe G. Ciarlet, The Finite Element Method for Elliptic Problems, Université Pierre et Marie Curie, Paris, France, 1974.
[37] S. Brenner, L. Scott, The Mathematical Theory of Finite Element Methods, third ed., in: Texts in Applied Mathematics, vol. 15, Springer, New York, 2008.
[38] R. Guo, T. Lin, Q. Zhuang, Improved error estimation for the partially penalized immersed finite element methods for elliptic interface problems, Int. J. Numer. Anal. Model. 16 (4) (2019) 575–589.
[39] E. Burman, S. Claus, P. Hansbo, M.G. Larson, A. Massing, CutFEM: Discretizing geometry and partial differential equations, Internat. J. Numer. Methods Engrg. 104 (2014) 472–501.
[40] H. Wei, Y. Huang, FEALPY: Finite Element Analysis Library in Python, XiangTan University, 2017-2024, https://github.com/weihuayi/fealpy.
[41] B. Hosseini, N. Nigam, J.M. Stockie, On regularizations of the Dirac delta distribution, J. Comput. Phys. 305 (2016) 423–447.
[42] A.K. Tornberg, Multi-dimensional quadrature of singular and discontinuous functions, BIT Numer. Math. 42 (2002) 644–699.
[43] P. Blanchard, E. Brüning, Mathematical Methods in Physics: Distributions, Hilbert Space Operators and Variational Methods, Birkhäuser, 2003.